UNIVERSITY OF TARTU
Faculty of Science and Technology
Institute of Chemistry

Karl-Sten Põder

HIGH ENERGY DENSITY Zn-ION HYBRID CAPACITOR USING NON-AQUEOUS ELECTROLYTES

Master's Thesis (30 ECTS)
Curricula: Materials and Processes for Sustainable Energetics

Supervisors: Assoc. Prof. Alar Jänes
Research Fellow Jaanus Eskusson

Tartu 2023

Kõrge energiatihedusega Zn-ioon hübriidkondensaator mittevesilahuselistes elektrolüütides

Intensiivseid teadusuuringuid superkondensaatorite valdkonnas on soodustanud vajadus suure tõhususega energiasalvestussüsteemide järele. Hübriidkondensaatorite eesmärk on vähendada akude ja elektriliste kaksikkihi kondensaatorite erinevust energiatiheduse osas. Uuringu eesmärgiks oli välja selgitada, kas Zn-ioon hübriidkondensaatoritel on vajalikud omadused, et olla alternatiivne tuleviku energiasalvestustehnoloogia.

Katsetati erinevaid atsetonitriili ja propüleen karbonaadi lahustite kombinatsioone koos $Zn(TFSI)_2$, $Zn(BF_4)_2$ ja $Zn(OTf)_2$ sooladega. Zn ja süsinikkangast elektroodi uuriti erinevate füüsikalise karakteriseerimise meetodite abil. Koostatud testrakkude elektrokeemilist toimivust mõõdeti ja võrreldi tsüklilise voltamperomeetria, elektrokeemilise impedants spektroskoopia, konstantse vooluga täis- ja tühjakslaadimise ning Ragone mõõtmiste abil. Atsetonitriili-põhised süsteemid näitasid paljulubavaid elektrokeemilisi tulemusi.

Märksõnad: Zn-ioon hübriidkondensaator, õhuke Zn elektrood, süsinikkangast elektrood, mittevesilahuseline elektrolüüt, kuloniline ja energia efektiivsus.

CERCS kood: P401 Elektrokeemia

High energy density Zn-ion hybrid capacitor using non-aqueous electrolytes

Intensive research in the field of supercapacitors has been fuelled by the need for high efficiency energy storage systems. The concept of hybrid capacitor aims to close the gap between batteries and electrical double-layer capacitors in terms of improving the energy density. The purpose of the study was to find out if Zn-ion hybrid capacitors have the necessary characteristics and properties to be alternative future energy storage technology.

Different combinations of acetonitrile and propylene carbonate solvents, together with $Zn(TFSI)_2$, $Zn(BF_4)_2$ and $Zn(OTf)_2$ salts were tested. Zn and carbon cloth electrode were studied using different physical characterization methods. Electrochemical performance for assembled test cells was measured and compared using cyclic voltammetry, electrochemical impedance spectroscopy, constant current charge/discharge methods and Ragone plots. Acetonitrile-based systems exhibited promising electrochemical results.

Keywords: Zn-ion hybrid supercapacitor, Zn thin foil electrode, fibrous carbon cloth electrode, non-aqueous electrolyte, coulombic and energy efficiency.

CERCS code: P401 Electrochemistry

Table of Contents

2. Abbreviations and Symbols

EDLC - electric double-layer capacitor
ESR - equivalent series resistance
ASC - asymmetrical supercapacitor
AC - activated carbon
PPy - polypyrrole
CNT - carbon nanotubes
LIB - lithium-ion battery
LIHC - lithium-ion capacitor
PVDF - poly-1,1-difluoroethene
NIB - sodium-ion battery
SEI - solid electrolyte interface
NIHC - sodium-ion capacitor
PC - propylene carbonate
PTCD -perylene tetracarboxylic dianhydride
PANI - polyaniline
EC - ethylene carbonate
DEC - diethyl carbonate
TNO - titanium niobium oxide
LNMO - lithium nickel manganese oxide
KIHC - potassium-ion capacitor
KTO - potassium titanium oxide
SHE - standard hydrogen electrode
DMC - dimethyl carbonate
EMC - ethyl methyl carbonate
CIHC - calcium-ion capacitor
MIHC - magnesium-ion capacitor
AIHC - aluminium-ion capacitor
PMC - propyl methyl carbonate
Et_4NBF_4 - tetraethylammonium tetrafluoroborate
AN - acetonitrile
γ-BL - γ-butyrolactone
PEO - poly(ethylene oxide)
RTIL - room-temperature ionic liquid
$BMImBF_4$ - 1-n-butyl-3-methylimidazolium tetrafluoroborate
(EMIM)Cl - 1-ethyl-3-methylimidazolium chloride
$Zn(TFSI)_2$ - zinc di[bis(trifluoromethylsulfonyl)imide]
$Zn(CF_3SO_3)_2$ or **$Zn(OTf)_2$** - zinc trifluoromethanesulfonate
PDA - polydopamine
LiTFSI – lithium bis(trifluoromethanesulfonyl)imide
ZIB - zinc-ion battery
DMF - N,N-dimethylformamide
G2 - diglyme
TMP - trimethyl phosphate
DES - deep-eutectic solvent
CV - cyclic voltammetry
CCCD - constant current charge/discharge method
EIS - electrochemical impedance spectroscopy
RS - raman spectroscopy
XRD - x-ray diffraction
BET - Brunauer-Emmett-Teller Theory
IUPAC - International Union of Pure and Applied Chemistry
SEM-EDS - scanning electron microscopy with energy dispersive spectroscopy
ZIHC - zinc-ion hybrid capacitor

3. Introduction

The growing need for more environmentally friendly and sustainable solutions in energy storage has led to intensive research in the field of supercapacitors. The development of high efficiency energy storage systems is gaining importance as these systems enable more efficient performance for stand-alone power applications and in turn reduce greenhouse gases, by slowing down energy depletion.

The concept of hybrid metal-ion capacitors is essentially a combination of a battery and a capacitor. The fundamental purpose of the hybrid capacitor is to try to close the gap between batteries in terms of improving the specific energy. Furthermore, having capacitive-type electrode in the system increases the lifetime and stability of hybrid capacitor devices compared to batteries. Multivalent metal ions (Mg^{2+}, Ca^{2+}, Zn^{2+} and Al^{3+}) hybrid capacitors have lately gained attention due to cost, abundance, and non-toxicity as metals. In addition, these metal ions have possibly great charge storage capabilities because of the multivalency, which gives them high volumetric capacitance and energy density. Therefore, the idea of zinc-ion hybrid capacitor holds a lot of promise of becoming a sustainable and cost efficient alternative in future energy storage technologies. Zinc is a non-toxic metal, has abundant reserves and very high volumetric capacitance of 5855 mA h cm^{-3}. In addition, it is already known that zinc-ion hybrid capacitors have good compatibility with aqueous electrolyte systems due to zinc's low redox potential (-0.76 V vs. SHE). Combining a hybrid capacitor device with non-aqueous electrolytes can further enhance the electrochemical performance of a supercapacitor due to the much larger potential window that can be achieved using organic electrolytes.

The aim of this thesis is to find out if Zn-ion hybrid capacitors have the necessary characteristics and properties to be applicable for commercial use. Particularly, 1) to achieve high energy density while using cheap electrode materials (Zn, carbon). 2) Wider potential window demonstrates good electrochemical performance. 3) Utilizing organic electrolyte improves cycle life for Zn-ion hybrid capacitors.

4. Literature Review

4.1 Electric Double-Layer Capacitors (EDLCs)

The electric-double layer hypothesis was introduced by Hermann von Helmholtz in 1853 and was later improved by Gouy and Chapman. EDLCs store energy electrostatically, a double-layer is formed in the electrolyte that is also called Helmholtz layer. A conventional EDLC has two electrodes separated by a separator, a positively charged (+) and negatively charged electrode (-) (Fig. 1). By cause of Coulomb's forces, the positively charged electrode attracts an equivalent number of opposite charges carried by ions in the electrolyte. To keep the balance of the system (electrical neutrality) a similar diffusion of positive charges takes place on the negatively charged electrode [1-3].

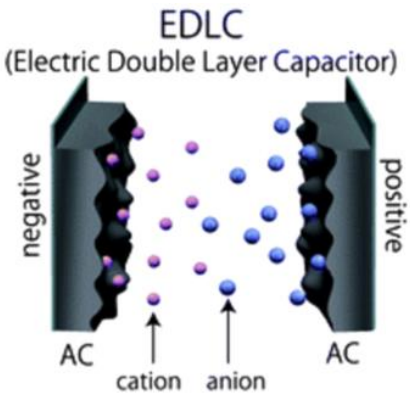

Figure 1. Symmetric EDLC cell design utilizing activated carbon (AC) for both (+) and (-) electrodes [1,76].

The electrolyte is one of the central components of EDLCs and consists of a solute dissolved in the solvent or pure salt (in the case of solvent-free ionic liquids [ILs]). The electrolyte plays an important role in the EDLC in several ways such as: (1) providing ionic conductivity and thus allowing for charge compensation on each electrode; (2) contributing to the formation of an electric double-layer; and (3) participating in the charge storage processes, i.e. reversible redox reactions in pseudocapacitors. Typical electrode materials for EDLCs are porous carbon-based materials because they have stable wide potential window in both aqueous and non-aqueous electrolyte solutions. Some more popular solvents for EDLCs are water, acetonitrile, propylene carbonate, mixture of different cyclic and linear carbonates, and ionic liquids [4]. However, with water-based solvents the maximum cell potential can be around 1.23 V. With the use of acetonitrile or some cyclic carbonates the electrode potential window can reach 3 V and with ionic liquids it is even possible to achieve 4 V [1].

Over the years a lot of emphasis has been put on developing new electrode materials to improve charge storage performance of EDLC. Electrode material fulfils one of the most influential roles in terms of the performance of a device. Therefore there are key properties that a potential electrode material must meet. To name a few: high specific surface area, well-developed micro- and mesoporosity, chemical and thermal stability, good electrical and heat conductivity, tailorable porosity, low-to-moderate costs, and ease of processability. For this

reason, the specific surface area of carbon material plays a crucial role and activated carbon is one of the most common electrode materials for EDLCs with the specific surface area of around 2000-2500 m^2 g^{-1}. In this case, capacitance of EDLC strongly depends on the pore size and the number of pores in the electrode material because the size of electrolyte ions must match with the pore size to be able to penetrate them and create a double-layer interface. Capacitance is one of the most important characteristics in rating supercapacitor performance [1].

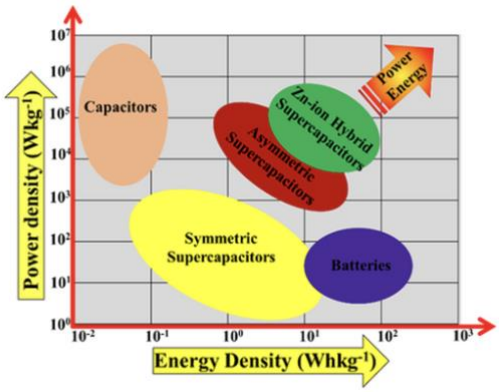

Figure 2. Ragone plots of different energy storage devices [1,77].

Another important performance characteristic for supercapacitors is ESR. It includes the resistance between current collectors and electrodes, the resistance in the electrode due to porosity and particulate nature of the composition, the resistance of the electrolyte and external load contact [1].

Specific energy and power densities are necessary parameters to measure and assess supercapacitors and to compare them against other electrochemical devices, which is usually done in a Ragone plot. The specific energy shows how much energy is stored in a supercapacitor, mostly measured in W h kg^{-1}. It is also reliant on the materials such as electrolyte, electrodes (porosities and particle sizes) and current collectors. Generally, for current collectors, light, electrochemically stable and conductive materials are desired. Moreover, changes in energy densities are also influenced by the interaction between electrode-electrolyte interface. It is reported that for EDLCs using graphene as a carbon material can deliver specific energy around 85 W h kg^{-1} at room temperature. This number is comparable to e.g., Ni-metal hydride batteries [5]. Power density shows how fast the stored energy in the supercapacitor can be released, normally measured in W kg^{-1}. Here again, reportedly graphene displays better power densities than other carbon materials, 40-250 W kg^{-1} [6, 7].

On utilization level, the performance of supercapacitors is established by the relationship of specific energy density and power density. An electrochemical device performs better, the higher are both densities. However, high energy density does not equal with high power density. For that reason, a Ragone plot is used to compare and assess different energy storage devices such as batteries, fuel cells, supercapacitors, and regular capacitors. In the Ragone plot, the specific energy density is plotted against the specific power density (Fig. 2). The figure indicates that normally supercapacitors have high power densities, but low energy densities, that is especially true for ELDCs. Other types of supercapacitors such as

pseudocapacitors and hybrid capacitors commonly differ in densities. Low energy density is one of the major challenges to overcome in the current supercapacitor industry [1].

Supercapacitors have a long cycle life, for example, EDLCs can sustain up to 100 000 or 1 000 000 cycles, whereas batteries have 10 to 100 times less cycles in their lifetime. High power densities allow supercapacitors to quickly release the stored energy, but lower energy densities than batteries mean that the amount of energy stored inside the EDLC is not very high. Finally, charging and discharging times for supercapacitors are in the range of seconds, with battery it takes a couple of hours to charge. Combining the abovementioned characteristics of a supercapacitor, more promising market penetration is possible in industries or applications where fast charging times and quick release of energy is needed [1].

4.2 Asymmetrical Supercapacitors (ASCs)

EDLCs show very long cycle life and high power densities ranging from 1 to 100 kW kg^{-1}. The problem for EDLCs lay in low energy densities, which limit the possibilities to use these devices. As a result of that, research focus has shifted to another direction to attempt to solve the energy density issue without compromising power and cycle life [8]. Thus, an alternative would be another type of supercapacitor called asymmetric supercapacitors. These are also categorized into two types, systems with two capacitive electrodes, where one electrode has a higher potential window than the other or hybrid capacitors, which are more battery-like devices. Hybrid capacitors contain an electrode which stores energy via faradaic processes and an electrode which cumulates charge coming from capacitive mechanism [8].

Different potential window allows higher cell operating potential during charging-discharging. Therefore, a well-designed asymmetric supercapacitor presents a great outlook for future purposes of aiming to boost the energy density for applications where energy storage with high power delivery is needed [9].

Aqueous capacitive RuO_2-based asymmetric supercapacitors have been studied already in 1999. The asymmetric supercapacitor, where expensive RuO_2 was utilized as the positive electrode reportedly reached average specific capacitance of 720 F g^{-1} at lower scan rates (2 mV s^{-1}), but capacitance dropped significantly with higher potential scan rate (50 mV s^{-1}) [10].

A replacement for ruthenium oxide can be found in MnO_2. It is an attractive choice considering its abundance, low cost, and high theoretical capacitance. The capacitance of MnO_2, 200 F g^{-1} is rather low compared to RuO_2, but energy densities are worthy of comparison because of high potential used in the asymmetric system [8]. The combination of

MnO_2 as a positive electrode and activated carbon as negative electrode favours the operating potential in aqueous electrolyte to be enhanced up to 2 V [11]. Wei et al. addressed that due to the pseudocapacitance happening at the surface or near the surface of the active material, the performance of MnO_2 is greatly influenced by the surface area, particle size and morphology [12]. Even though MnO_2 is deemed to be an appealing pseudocapacitive material, its insufficient conductivity (10^{-5} to 10^{-6} S cm^{-1}) is a critical restraint to obtain good specific capacitance values, cycle life and rate capability [8].

The second type of asymmetric supercapacitors are hybrid capacitors, where one of the electrodes stores energy by faradaic processes and the other uses capacitive mechanism for charge cumulation. Furthermore, hybrid capacitors can be classified as battery/capacitors (aqueous hybrid capacitors) such as $Ni(OH)_2$//AC or PbO_2/AC, redox-electrolyte capacitors, or metal-ion capacitors ($Li_4Ti_5O_{12}$ and Li_2MoO_3), which are commonly also combined with activated carbon as the negative electrode. These supercapacitors are of particular interest because of their cost and very high theoretical capacitance.

Aqueous hybrid capacitors using metal oxide-based electrodes can achieve higher energy densities than carbon-based symmetric capacitors. The cell potential can overcome 1 V due to the pairing of two different types of electrodes [8, 13].

For metal hydroxide-based electrodes, transition-metal hydroxides such as $Ni(OH)_2$ and $Co(OH)_2$ are mostly studied because of their electrochemical characteristics. A hybrid capacitor was developed by using $Ni(OH)_2$ as a positive electrode and activated carbon as the negative electrode [14, 15].

Another class of hybrid capacitors contains mixed transition-metal based electrodes such as nickel-cobalt or nickel-molybdenum oxides and cobalt-nickel sulphides [8]. With AC as the negative electrode, the supercapacitor achieved a potential window of 1.6 V [16]. Recently, metal sulphides have gained a lot of attention to potentially be another promising electrode material for hybrid capacitors. The reason behind it is that compared to metal oxides, better mechanical and thermal stability, electrical conductivity, and greater electrochemical activity have been reported. One way to increase the conductivity of a metal oxide electrode is to combine it with a conducting polymer [8, 17].

Low conductivity levels of battery-type and pseudocapacitive materials restrict charge transport properties and display low power densities. Efforts are now focused on making electrodes with better electrical conductivity and kinetics. For this reason, composite electrodes are being intensively studied, to combine materials such as carbon fibres, graphene, and carbon nanotubes together with a battery-type material [8]. Moreover, sulphide-based redox systems

could be another direction to aim for. Mixing $NiCo_2S_4$ nanosheets with N-doped carbon foams in 6 M KOH electrolyte solution demonstrated a capacitance of 877 F g^{-1} at 20 A g^{-1} [18]. Another system made from NiS/CNTs as the positive electrode and graphene as the negative electrode was investigated [19]. Combining faradaic materials with conductive carbon materials is an interesting way of enhancing electrical conductivity to increase the cycling stability, power density of hybrid capacitor systems [8].

Redox electrode-based capacitive systems are another category of aqueous asymmetric supercapacitors with pseudocapacitive electrodes. Mainly, for aqueous electrolyte hybrid capacitors, negative electrodes are carbon-based EDLC electrodes with lower specific capacitances compared to faradaic-type electrodes. Therefore, it is achievable to have a system with higher energy density when changing carbon-based EDLC negative electrode for the Faradaic electrode [8].

Some pseudocapacitive materials such as MoO_3, VN (vanadium nitride), Bi_2O_3, V_2O_5 and Fe_3O_4 can operate in a negative potential range and have better specific capacitances than carbon-based materials [8, 20].

Due to V_2O_5 potential window and several oxidation states (II-V), it is another candidate for the negative electrode. Although, it is difficult for pure V_2O_5 systems to have good cycling stability because of its dissolution in aqueous electrolytes and weak electronic conductivity [8]. A hybrid system with PPy/V_2O_5 material was built to enhance conductivity and limit the dissolution of the oxide. The system reached 10 000 cycles and lost only 5% of its capacitance compared to almost 18% capacitance loss in V_2O_5/AC supercapacitor [21].

4.3 Capacitive-Type Electrode Materials

The most popular choice of capacitive-type electrode material is activated carbon. Some great sources of activated carbon include wood, carbohydrates, natural fibres, and bone char. This material is preferred because of its easy synthesis process, low manufacturing cost and coefficient of thermal expansion, as well as thermal stability. Nevertheless, activated carbons do need additional conducting materials like carbon black to overcome initial low electronic conductivity [4]. Recent rise of renewable materials has also introduced a potential new electrode material candidate such as biomass-derived ACs (from banana peels or coconut shells etc.). All alkali metals described in this section basically use the same capacitive electrode materials. Activated carbon is the most widely used material for LIHCs, NIHCs and KIHCs, but graphene and CNTs are also possible to utilize in these systems. Because of

electrolyte consuming mechanism in NIHCs, AC is doped with boron or nitrogen to boost electrochemical performance. Thus far, for calcium-ion capacitors AC is the only choice. There is limited amount of studies made due to difficulty of controlling the movement of Ca^{2+} adsorption to AC [4].

MIHCs have possibilities to utilize graphene, CNTs etc. for the capacitive electrode, but more investigation is needed to see how well Mg^{2+} absorbs into those materials. Because Mg forms stage 1 graphite intercalation compound, graphite would be a poor choice of electrode material [4].

4.4 Choice of Electrolytes for Metal-Ion Capacitors

Electrolytes are one of the most important parts of the electrochemical storage systems. They should have a high dielectric constant and ionic conductivity to minimize the rate of self-discharge and to initiate fast ion transportation. To avoid electrolyte degradation and reach good specific energy values, the stability window of the electrochemical cell should be high enough. Furthermore, it is important to have a stable electrochemical connection between the other cell components such as electrodes, current collectors, and the separator. Lastly, the electrolyte should be non-toxic, non-hazardous, and environmentally friendly [4]. In comparison to non-aqueous electrolytes, aqueous electrolytes have greater ionic concentration/conductivity and smaller solvated ions. In addition, they are safe, low cost, non-flammable, easy to synthesize and have low viscosity. The limitation with aqueous electrolytes is the operating potential window, which is around 1.23 V. For non-aqueous electrolytes and ionic liquids it can be 3 V and 4 V, respectively. Consideration of radii of cations and anions and the ionic conductivity are essential for selecting the right electrolyte [4].

Electrolytes have an important component such as an organic solvent, which should have a good solubility constant and a low viscosity for fast motion of ions. Typical organic solvents for LIHCs are ethers, EC, PC and EMC/ DMC/ PMC carbonates [22]. These solvents need a salt to obtain the ionic conductivity of electrolytes [4].

It is important for Li salts to be low cost, safe, non-toxic, non-flammable and environmentally friendly. Furthermore, the cation-anion asymmetry of the salt shall not be big enough to influence the capacity of the system. A weak affinity toward lithium cation is preferred for the negative ion of the salt and high degree of polarity is desired to help dissolve the salt in the solvent [4]. For aqueous-based LIHCs, most widespread salts are LiOH, LiCl and Li_2SO_4. Most LIHCs use organic electrolytes because water and oxygen react with lithium and non-aqueous

electrolytes have much higher potential window than aqueous based. Some more common inorganic and organic salts for LIHCs are $LiPF_6$, $LiAsF_6$, $LiBF_4$ and $LiClO_4$, $LiB(C_2O_4)_2$, $LiP(C_6H_4O_2)_3$, Et_4NBF_4 and $LiSO_3CF_3$ [22].

NIHCs have a poor selection of available electrolytes, mainly organic or aprotic. Although, basically it is possible to use aqueous systems as well, including salts such as NaOH, NaCl, Na_2SO_4 and $NaNO_3$. One additional salt is $NaClO_4$, it has a high solubility in water which allows to have a high concentration IL-kind system. For organic electrolytes, Na-salts i.e. $NaPF_6$ and $NaBF_4$ are utilized, with the addition of some ether-based solvents which are estimated to give good electrochemical performance due to the compatibility of graphite [23].

KIHCs use electrolytes comparable to LIHCs and NIHCs. It is feasible to have both aqueous and non-aqueous systems in KIHCs. In case of aqueous electrolytes, the same salts are implemented as in LIHCs and NIHCs and organic electrolytes have analogous salts to both lithium and sodium [4].

The problem with CIHCs is that Ca^{2+} cannot penetrate through the SEI layer and the dissolution and recovery of calcium have not been detected. Experiments were done by dissolving $Ca(ClO_4)_2$ in AN, PC and γ-BL [24].

Aqueous based Mg-ion systems use Mg^{2+}-ion sources like $MgSO_4$, $Mg(NO_3)_2$ or $MgCl_2$. Mg does not react with ethereal solvents; thus, these are preferred choices. Additional choices could be polymeric gel electrolytes and ILs. These electrolytes such as PEO eliminate cell leakage problem. RTILs have been studied as possible solvents for Mg salts to lessen the use of ethereal electrolytes (highly volatile and flammable) and to increase the solubility of Mg salts [24].

Up to now, for AIHCs a RTIL such as [EMIM]Cl mixed with $AlCl_3$ is regarded as the most advanced electrolyte due to Al's inclination towards chlorides. Both the Al salt and the chloride ion are considered as the ion source in that electrolyte solution [25]. In addition, aqueous electrolyte-based salts like $AlCl_3$ or $Al_2(SO_4)_3$ have been extensively utilized due to their non-toxic, easy-to-use, and low cost characteristics. Although, it should be mentioned that in aqueous systems Al_2O_3 layer forms which means that hydrogen evolution prevents the reversible deposition of Al^{3+}. That leads to poor efficiency values for Al electrode [4].

4.5 Hybrid Metal-Ion Capacitors

The idea of hybrid metal-ion capacitors is to combine an EDLC which can have a cycle life up to 1 000 000 cycles together with a rechargeable battery that has approximately 2 000

charge-discharge cycles. Hence, these hybrid devices in the best case scenario should be able to achieve at least 10 000 or more cycles without any degradation in the system. The importance of selecting a suitable positive electrode is vital to reach close to the cycle life of EDLCs [4].

Presently, the most well-known and attractive choice of all the metal-ion systems is Li-ion technology which is leading the battery industry [26]. However, cost, recyclability and the overall need for Li is growing because it is a non-renewable resource, the focus has shifted to alternative metal-ion possibilities [4].

4.5.1 Monovalent Metal-Ion Capacitors

Thus far, Li-ion technology is the most popular choice in the battery industry because of the high specific energy and the fact that other alternative metal-ions have not shown better operating potential window and electrochemical stability. Since, the focus of metal-ion hybrid capacitors is to achieve longer lifetime than batteries and better energy densities than EDLCs or ASCs, the first step in this area was to try and combine the current Li-ion battery technology with an EDLC-type electrode [4]. LIHCs have many benefits compared to LIBs and EDLCs. There is a big safety advantage over LIBs due to better mechanical and thermal stability as well as improved short-circuit protection because these hybrid storage systems do not contain oxygen, which can lead to ignition or explosion if the internal pressure of the cell increases. Furthermore, the operating potential window for LIHCs is equal to the LIBs due to the battery electrode. Lastly, because of the higher capacitance of LIHCs compared to EDLCs, the energy density is better [4].

Metal oxides generally possess low electronic conductivity, which reduces the power density of LIHCs containing TiO_2 as the faradaic electrode. As a result of that, TiO_2 is mixed with binders (i.e., PVDF) and conducting carbon powders to address that problem. LIHC having anatase phase TiO_2 as the battery electrode displayed a specific power of 9.45 kW kg^{-1} and specific energy of 31.5 W h kg^{-1} [27]. Xu et al. reported that using $Li_4Ti_5O_{12}$-graphene as the battery electrode and AC as EDLC electrode yielded the energy density of 30 W h kg^{-1} and the power density of 1 000 W kg^{-1} with a potential window of 1.0-2.5 V [28]. Apart from titanium oxide compounds, there are also possibilities with Fe_2O_3/Fe_3O_4 and SnO_2 [22, 29].

Pseudocapacitive metal oxides such as V_2O_5 and Nb_2O_5 are not exactly battery-type materials. Lim et al. showed that a system consisting of a battery electrode made from a mixture of mesoporous carbon-Nb_2O_5 and a capacitive electrode of AC demonstrated a specific energy

of 74 W h kg^{-1}. Although, most likely due to low electronic conductivity of Nb_2O_5 the specific power was poor (120 W kg^{-1}) [30]. In addition, a V_2O_5/CNT nanocomposite LIHC system with AC as the capacitive electrode exhibited the maximum energy density of 40 W h kg^{-1} at 210 W kg^{-1} [31]. MXenes consist of a vast number of layered transition metal carbides/carbonitrides, which reportedly display ideal intercalation reactions for metal-ion capacitors [32].

The last class of battery-type electrodes are Si-based materials. Even though, Si has a very high intercalation capacity, it is also considered to be one of serious deficiencies of Si. Lithiation causes it to increase over three times in volume, which disturbs the capacity of Si-based battery type electrodes. Yi et al. investigated a LIHC system of B-doped Si/SiO_2/C battery electrode and a capacitive electrode made from porous spherical carbon. The specific energy and power were 128 W h kg^{-1} and 1.23 kW kg^{-1} respectively. After 6 000 cycles, the device had a capacitance retention of 70% [33].

There are a few advantages that Na-based compounds have over Li-based compounds. When talking about batteries, data analysis has reportedly shown better thermal stability and depth-of-discharge for NIBs than for LIBs [34]. Moreover, Na-ion systems have much wider choice of raw materials to prepare Na-ion electrodes, for example, rock salt, Na_2CO_3 and sea salt. For current collectors, Na-based systems allow the usage of Al for both electrodes.

Transition metal sulphides/selenides are a type of electrodes employed in NIHCs. $MoSe_2$ is a compound that have been studied as the negative electrode in NIHC. To increase the electrochemical performance of transition metal selenides usually conductive carbon additives are incorporated into the electrode material. The system of $MoSe_2$ with carbon nanospheres as negative electrode in 1 M $NaClO_4$ in PC electrolyte solution was constructed and showed capacity of 348 mA h g^{-1} at 4.0 A g^{-1} after 120 cycles [35].

Organic compounds are cheaper and easier to synthesize than inorganic materials. A NIHC system was assembled having PTCD as battery electrode and PANI as capacitive electrode. The capacitor displayed a specific energy of 95 W h kg^{-1} and a specific power of 7 kW kg^{-1} [36]. Ti and Nb-based compounds as electrode materials are also worth consideration. To increase the energy density of the system, mixing these two metal oxides together have exhibited interesting results for NIHCs [37].

Electrochemical performance for K-based system is to some extent proportionate to Na-ion systems, and it also has some advantages over Li-based systems. As is the case with Na, the amount of K resources compared to the availability of Li is a big factor. Like Na, K does not react with Al and a K-salt is much cheaper than Li-salt. The cell potential of K-ion system is almost comparable to Li-ion system because the standard redox potential is only

slightly higher than Li's, -2.93 V to -3.04 V. Unfortunately, due to K-ion's larger size and higher mass compared to Li-ion, KIHCs have quite low volumetric and gravimetric energy vs LIHCs [4].

Mixture of Ti-oxides and MXenes have showed promising long-term cyclability and capacity retention values. The system was synthesized by treating Ti_3C_2 MXene in KOH solution in the presence of H_2O_2 and M-KTO ($K_2Ti_4O_9$) nanoribbons as negative electrode was produced. Electrochemical testing was conducted in 1 M KPF_6 electrolyte solution. K-ion based system achieved a capacity of 151 mA h g^{-1} at 50 mA g^{-1} [38].

A metal phosphide compound Co_2P mixed with rGO as negative electrode and AC positive electrode demonstrated a specific energy of 87 W h kg^{-1} and power density of 4 260 W kg^{-1} with maximum potential of 4 V [39].

Moreover, polyanions, alloying-type electrodes and organic compounds have also been researched. Alloying-type electrodes are mainly implemented to improve capacity degradation, but these systems still showed some pulverization of electrodes and electrolyte deterioration, as well as considerable volume expansion and low conductivity (for K_xP_y compounds) [40-42].

4.5.2 Multivalent Metal-Ion Capacitors

Thus far, there have not been any remarkable progress being made in the field of CIHC. There are various limitations which have disrupted the development phase. For example, finding a fitting electrolyte solution, formation of impermeable SEI layer and minimal choice of electrode materials. It should also be mentioned for comparison reasons that the SEI formation in Li favours the Li-ion diffusion but is not the case with Ca. However, nowadays cost effectiveness usually makes a strong argument in favour of using some material. There are abundant resources of Ca available, and Ca has a standard redox potential of -2.87 V (vs. SHE). Moreover, Ca has a good biocompatibility, which can make Ca-based energy storage systems the safest technologies to date [4].

Alloying-type electrode materials have reportedly demonstrated positive performances. Ca and Sn alloying method was used to combine dual ion battery electrode with graphite as the capacitive electrode in the system. The solvent for this calcium ion battery system (Sn/$CaPF_6$/graphite) utilized a combination of four different carbonates (EC/PC/DMC/EMC). Cycling stability measurements at 100 mA g^{-1} for 350 cycles showed coulombic efficiency of 95%, achieving average potential of ~4.1 V [43]. In addition, some hexacyanoferrates in aqueous systems have displayed decent storage characteristics. CuHCF was used as electrodes

in super concentrated 8.37 M aqueous $Ca(NO_3)_2$ electrolyte solution at 2 C during 150 cycles [44].

MIBs are appealing due to Mg's low reduction potential of -2.37 V (vs. SHE) and volumetric capacity of 3 833 mA h cm^{-3}, which is much higher than Li's 2 062 mA h cm^{-3} [24]. In addition, Mg does not form the SEI layer, while still going through the plating reaction which means that dendritic growth on the negative electrode does not take place. Regardless of the encouraging characteristics, MIBs are short of proper positive electrode materials where Mg-ion can diffuse with fast kinetics, along with poor matching of electrolytes with electrodes [4].

Transition metal chalcogenides and metal oxides are two possibilities for a battery-type electrodes in MIHCs. Former are acknowledged as good ion intercalation/deintercalation compounds and latter are popular because they can endure lattice strain when intercalation occurs and have strong structure. In addition, polyanion compounds which are members of pyrophosphate group offer improved chemical stability for positive electrodes [4]. Lastly, S was discovered to be a good intercalation material in Li-S systems [45].

Al is inert towards O_2 and moisture because it forms a protective layer at the metal-air interface, which allows it to be utilized in its pure metallic form as an electrode. The ionic size of Al-ion is the smallest among all metal ions and the volumetric specific energy is about 8 046 mA h cm^{-3} [4, 24]. As was discussed above, generally some significant knowledge should be had from the corresponding metal-ion battery systems to effectively try to develop capacitor devices.

A study was conducted to see the performance characteristics of an electrochemical system of TiO_2 nanotube array electrode with intercalated Al-ions in aqueous $AlCl_3$ solution [46, 47].

4.6 Zn-Ion Hybrid Capacitors

ZIHCs (Fig. 3) are gaining more research focus due to its theoretical capacity of 820 mA h g^{-1}, low cost, standard potential (-0.76 V vs SHE) and eco-friendliness [48, 49]. Contrary to the alkali and alkaline earth metals, Zn is the only metal that is stable in aqueous electrolyte environments in its pure metallic form. Moreover, it is non-flammable, non-

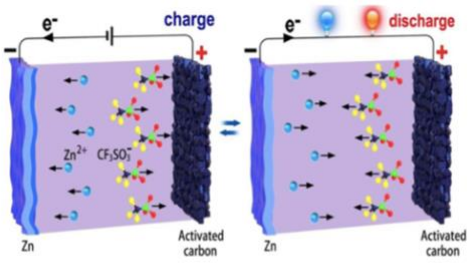

Figure 3. Schematic illustration of the device construction and working mechanism of the Zn-ion hybrid capacitor [1,75].

toxic and is not corrosive. Even though, Zn's ionic radius is smaller than Li's, the ion diffusion in a Zn-based system is a slow-moving process and Zn-ions do not easily get absorbed on the capacitive electrode. Zn's high standard electrode potential (-0.76 V vs. SHE) results in a quite modest specific energy performance and cell potential limitation. Combination of all the above mentioned aspects have thus far prevented its usage in hybrid capacitors. To actualize ZIHCs, it is important to find a fitting capacitive electrode material. Despite the disadvantages, Zn has a volumetric capacity of 5 851 mA h cm^{-3} and a stable electrode-electrolyte interface which still makes it worthwhile to research and investigate ZIHCs [4, 49].

4.6.1 Battery-Type Electrode

Zn can be employed directly in metallic form as a battery-type electrode in aqueous electrolytes because of its low redox potential and stability in humidity and air. However, at high current densities ZIHCs suffer from nucleation and Zn dendrite growth, which inhibits reaching favourable specific power values. Dendrite formation influences the cycling stability and when dendrites pierce separator, it leads to possible short-circuit and overall failure of the device. This problem has been observed more in alkaline electrolytes than in mildly acidic or neutral electrolytes [50]. In alkaline electrolytes, the formation of $Zn(OH)_4^{2-}$ ions occurs, and they start to unevenly decompose on the surface of the Zn electrode [51]. Therefore, electrolytes such as $ZnSO_4$, $Zn(TFSI)_2$ and $Zn(CF_3SO_3)_2$ are preferred in ZIHCs [49].

Another complication in ZIHCs is the metal corrosion, which mostly develops in $ZnSO_4$ and $Zn(TFSI)_2$. Constant contact between the negative electrode and the electrolyte results in a poor lifetime for ZIHCs due to corrosion reactions occurring inside the cell. In both electrolytes, there is also a worry of internal pressure increase and danger of explosion because of H_2 evolution which follows Zn corrosion [49, 52]. To use ZIHCs in practical applications it is important to improve the chemical resistivity of Zn electrode. Significant efforts should be directed to the negative electrode design such as 3D Zn networks or graphite fibres as substrates for layered Zn sheets [53, 54]. Furthermore, surface modification i.e., CNT scaffolds on Zn foil can be another solution because it restricts Zn dendrite growth during Zn plating/stripping [55].

Electrolyte additives are another option for improving the performance of ZIHCs. One effective method is to increase the salt concentration in the electrolyte. For example, a 7.5 M $ZnCl_2$ aqueous electrolyte solution solved Zn plating/stripping issue and had a capacity retention of 95% after 100 000 cycles. The achieved energy density was 217 W h kg^{-1} at the power density of 450 W kg^{-1} [56]. Nevertheless, it is recommended to adjust the salt

concentration in way that it would still be low cost and not have significant reduction in ionic conductivity or rate capability [49]. Organic additives like polymers and surfactants have also reportedly lowered corrosion rate and dendrite growth in the device [57].

4.6.2 Capacitive Electrode Materials

Commonly in ZIHCs, carbonaceous materials are utilized in the positive electrode. Carbon-based materials are considered cheap and sustainable green materials. In energy storage systems they are extensively employed because of their high surface area and electronic conductivity, as well as high electrochemical stability. Nevertheless, carbonaceous cathodes still need some modifications to improve their charge storage capabilities [49].

AC can be modified by different mechanisms to further improve charge storage capabilities (capacity). One way is to manipulate with the specific surface area properties and pore structure of AC, via changing the pyrolysis temperature or adding new precursors during carbon material synthesis process [49]. Another method is to use heteroatom doping. Including foreign atoms to carbon electrodes increase electronic conductivity due to better electrolyte infiltration and greater number of active sites [58]. Lastly, for carbon materials there is also an opportunity to include pseudocapacitance for better charge storage performances. Hence, the addition of oxygen-based functional groups such as carboxyl (-COOH) and hydroxyl (-OH) improves the specific energy and capacity of ZIHCs [59]. Even though, mostly the combination of Zn metal negative electrode and carbon-based positive electrode is used in ZIHCs, there have also been studies to utilize non-carbon positive electrodes like metal oxides, MXenes, organic polymers and phosphorenes [49].

A ZIHC system having MnO_2 nanorods coupled with AC as the positive electrode in 2 M $ZnSO_4$ aqueous electrolyte demonstrated a specific energy of ~59 W h kg^{-1} and a capacity of 83.8 mA h g^{-1} [60]. MXenes offer increased electrical conductivity and hydrophilicity, but at the same time give up porosity [49, 61]. Polymer materials are also one possibility for ZIHC electrodes. PDA was added on porous carbon cloth substrate to replace the Zn-based electrode. The device reportedly showed at 10 mA cm^{-2} a specific capacity of 0.58 mA h cm^2 in 2 M $ZnSO_4$ aqueous solution [62]. A study was conducted to incorporate few-layer phosphorene into the ZIHC device. The system was measured in two different electrolytes – in aqueous solution, 21 M LiTFSI + 1 M $Zn(SO_3CF_3)_2$ and in organic solution 0.2 M $ZnCl_2$ in Et_4NBF_4/PC. The investigation concluded that due to lower ionic conductivity in organic electrolyte the rate performance (<50% retention after 9 500 cycles) was not as good as in aqueous solution and at

higher current densities (6.4 A g^{-1}), the cell only exhibited 46.1 F g^{-1} of capacitance [63]. In conclusion, a lot more research needs to be done to achieve superior capacities and energy densities compared to current studies [49].

4.6.3 Electrolytes for Zn-Ion Hybrid Capacitors

Thus far, non-aqueous based electrolyte solutions have not been very extensively studied in supercapacitor systems as compared to aqueous solutions. As was already discussed in above sections, generally the development of metal-ion capacitor system starts from corresponding battery system configuration [4]. Therefore, some conclusions can already be made while reviewing organic electrolytes in ZIBs and their electrochemical performance. It is already believed that perhaps non-aqueous electrolytes can solve these fundamental electrochemical challenges such as Zn corrosion or dendrite growth that we currently see in ZIBs and ZIHCs [49]. Among organic electrolytes there are also RTILs and DESs (which are just another type of RTIL) [64].

Organic solvents such as AN, PC, DMF and G2 have thus far gained the most attention because of their high ionic conductivity, wide operation potential window and non-corrosive characteristics. Some Zn-salts to combine these solvents with include $Zn(TFSI)_2$, $Zn(OTf)_2$, $Zn(PF_6)_2$ and $Zn(BF_4)_2$. Han et al., investigated abovementioned solvents with these four zinc salts. DMF and G2 had anodic stability (vs Zn/Zn^{2+}) in the range of ~2.3 V to ~2.9 V compared to AN and PC, which had anodic stabilities of ~3.3 V to ~3.8 V. In addition, solutions using AN and PC achieved a coulombic efficiency of ~99% [65]. AN-based electrolyte solutions in 0.5 M $Zn(TFSI)_2$ and 0.5 M $Zn(CF_3SO_3)_2$ achieved Zn plating coulombic efficiency over 99% after 500 cycles at current densities of 1.25 and 10 mA cm^{-2} [66]. Ma et al. found that 0.5 M $Zn(TFSI)_2$ in PC exhibited coulombic efficiency of 98% at 2.5 mA cm^{-2}, but the electrolyte still contained Zn dendrites [67]. Ether-based solvent G2 in different zinc salts such as $Zn(TFSI)_2$, $Zn(OTf)_2$, $Zn(PF_6)_2$ reportedly developed additional redox reactions during Zn plating/stripping [65]. Another study was made by mixing two solvents, TMP was mixed with DMF as a co-solvent in 1:1 ratio, forming 0.5 M $Zn(OTf)_2$/TMP/DMF (1:1). This method improved cycling stability and rate capability in ZIB system [68].

RTILs and DESs have not drawn much attention yet. The main reason behind it is that RTILs have not exhibited very good reversibility when in cycling. DES electrolytes are being studied because they are environmentally friendlier choices compared to classical RTILs [64].

5. Methods

5.1 Raman Spectroscopy

A useful method to evaluate and define different materials and compounds is RS to measure vibrational spectra. RS provides data about almost all molecular samples and can be used to test solids, gases, and aqueous states. It is also good for classifying and pinpointing different materials through their characteristic peaks that various mixtures and compounds exhibit. However, it is not applicable for metals and its alloys because there exist no spectra for metals. For example, in the case of Zn-ion hybrid capacitors, it is not possible to analyse the spectrum of zinc but is very important for investigating the capacitive carbon electrode material [69]. The technique applies Raman scattering or effect which is photon interaction with the electron cloud of the material during measuring inelastic scattering . The molecules in the sample absorb photons and move to excited energy state. Afterwards, re-emission of photons of different wavelengths occurs and the molecule reverts to a different vibrational state than its initial ground state [1].

The analysis of Raman spectrum of some material contains plenty of information about its mixture. For instance, the position of peaks indicates its composition, and the intensity of peaks display relative amount of components in the compound. An indication of any stresses happening inside materials is usually observable when peaks have shifted from their characteristic peaks. Lastly, linewidth of peaks describes any defects, crystal quality, size, etc [69]. Carbonaceous materials generally show 2 peaks in the range of visible light (400-800 nm) and near-infrared (800-2500 nm). Disorder peak (D-band) is usually around 1350 cm^{-1} on the wavenumber and graphitic peak (G-band) occurs on the wavenumber of about 1590 cm^{-1}. D-band appears only when the structure of the material is amorphous. The higher is the intensity of the peak the more amorphous is the material [70].

5.2 X-Ray Diffraction

XRD is a popular tool implemented for determining and investigating unidentified crystalline materials. The idea is to bombard a sample with an x-ray beam via non-destructive way to evaluate diffracted and transmitted beams. It helps to detect the orientation of single crystals or grains as well as the structure of the sample. Furthermore, XRD can determine purity and texture of the sample and measure atoms distribution between the layers. The key parameters to study the sample against materials database or to calculate data about the sample,

are the angles of diffracted x-rays, intensity, and peak widths of the spectrum. The best results are obtainable when the sample is homogenous or single-phase. It is not possible to identify amorphous materials [1].

5.3 Brunauer-Emmett-Teller Theory

Low temperature N_2 sorption method based on BET theory is employed to identify specific surface areas of electrode materials like activated carbon and graphene. Surface area and pore size are both essential parameters in finding out material capacitance. This approach determines accurate specific surface area measurements by investigating the absorption isotherm of carbon dioxide, nitrogen, or argon gas in comparison to a reference cell. Electrochemical effectiveness of an active material when matched with an electrolyte is estimated via pore size measurements. In addition, the information about specific surface area and pore size are usually good for estimating any possible structural changes after heat or chemical treatment. The examination of absorption and desorption isotherms gives total specific surface area, which is generally given in $m^2\ g^{-1}$. Moreover, these isotherms help to identify pore size distribution [1]. According to the IUPAC, pore widths are categorized as micro-, meso- and macropores. Micropore widths are less than 2 nm, mesopores are between 2-50 nm and macropores are greater than 50 nm [71].

5.4 Cyclic Voltammetry

CV is used to measure how current density and capacitance values change at different potential scan rates. This technique helps to examine electrochemical behaviour of a test cell. Specifically applied to acquire data about electrochemical reactions together with kinetics, reaction reversibility and electrocatalytical processes. The analysis is generally conducted in a three-electrode configuration or electrochemical cell consisting of a working electrode, counter electrode, and reference electrode. In addition, it is also possible to carry out this measurement using a two-electrode test cell. It should be mentioned that if these two electrodes are different then it is better to use three-electrode system to get information about single electrodes. The electrode potential is controlled by a potentiostat. During CV measurement, the potential of the working electrode is measured against the reference electrode via linear back and forth scanning between the upper and lower specified potential limits [1]. Gravimetric capacitance values are calculated from CV data as stated in equation (1):

$$C = i \left(\frac{dE}{dt}\right)^{-1} \quad (1)$$

where E is the cell potential (in V or mV units), i is the current density (in A cm^{-2} units) and t is the time (in s or ms units). This equation can only be applied at low potential scan rates because of the small influence of ohmic drop [72]. The discharge and charge capacitances are calculated in accordance with equation (2):

$$C = \frac{\int_{\Delta E_1}^{\Delta E_2} j dt}{d(\Delta E)} \quad (2)$$

where j is current density, dt is time and ΔE is the cell potential.

Different potential scan rates are usually applied to measure how much capacitance values are affected. At lower scan rates supercapacitors mostly exhibit capacitive behaviour, when increasing the scan rate the specific capacitance decreases. Although, a high charging-discharging rate without any loss of capacitance is generally favoured in supercapacitors, at high scan rates ion transport to carbon pores is hindered due to slow-moving ion transport inside the electrode structure [1].

5.5 Constant Current Charge/Discharge Method

The second approach is utilized to learn about performance (power density and energy density), capacitance, equivalent series resistance and cycle life of a supercapacitor. CCCD is carried out by applying a constant current to a test cell and recording charge-discharge cycle times to measure its potential. The registered potential varies as a function of time with an applied constant current [1]. Generally, the efficiency of supercapacitor is shown as coulombic efficiency which is based on charge and discharge time values. That can often be deceptive because of the linear response it delivers. For example, in the case of a supercapacitor that stores energy electrochemically by faradaic reactions. Thus, it is better to use energy efficiency (η_{en}) parameter since it acknowledges the non-linearity of these CCCD curves by finding the ratio of areas under the constant discharge (CD) vs constant charge (CC) curve [73]. η_{en} is calculated via integrating constant current charge / discharge curves and then energy densities stored (E_{in}) and released (E_{out}) are calculated by equation (3):

$$E_{in,out} = i \int_{t(\Delta E_{min})}^{t(\Delta E_{max})} \Delta E(t) dt \quad (3)$$

where t is time (s), E_{max} and E_{min} are maximal and minimal cell potentials applied. The energy efficiency (η_{en}) is calculated via equation (4):

$$\eta_{en} = \frac{EN_{out}}{EN_{in}} \times 100\% \quad (4)$$

where EN_{out} is the energy released and EN_{in} is the energy stored during constant current charging cycle [73].

As is the case with CV, changing current densities during measurements allows to analyse mass transfer kinetics of electrodes. It is already known from cyclic voltammetry that capacitance values decrease with increasing current density [1].

Constant current charge-discharge method is also a good way to measure cycle life and investigate the deterioration of a supercapacitor by charging-discharging it over many cycles. Nowadays popular lithium ion batteries exhibit a lifetime of around 1000-2000 cycles. In comparison, supercapacitors can reach as high as 100 000 cycles for EDLCs or around 20 000 cycles for hybrid capacitors. During cycling, a supercapacitor gradually will lose its capacitance and equivalent series resistance will increase, which leads to losses in energy and power density. Finally, the degradation rate can be calculated from the data received from the cycling test, which is important knowledge for practical applications [1].

5.6 Electrochemical Impedance Spectroscopy

The third method is EIS which uses small magnitude alternating perturbation (usually potential, but current can be used as well). It can be averaged over long term because the response is continually stable. This method is used to analyse electrical characteristics of a supercapacitor cell by applying a range of different ac frequencies or time. EIS is useful for determining materials for designing or developing a supercapacitors and other energy storage devices [1].

The perturbation is generally applied as a sinusoidal wave function in a phasor diagram. $Z(\omega)$ is also called complex impedance because it can be described as a complex number of the vector sum of real Z' and imaginary Z'' parts [70]:

$$Z(\omega) = Z'(\omega) + Z''(\omega) \quad (5)$$

In the phasor diagram the two rotating vectors current (I) and potential (V) are separated by phase angle φ. For an ideal capacitor, the φ value is -90°. The phase angle can be calculated via equation (6):

$$\varphi(\omega) = \arctan\left[\frac{Z''(\omega)}{Z'\omega)}\right] \quad (6)$$

With data from EIS, series resistance R_s, series capacitance C_s, parallel resistance R_p and parallel capacitance C_p can be calculated via respective equations (7) - (10):

$$R_s = Z'(\omega) \quad (7)$$

$$C_s = -\frac{1}{\omega Z''(\omega)} \quad (8)$$

$$R_p(\omega) = \frac{|Z(\omega)|^2}{Z'(\omega)} \quad (9)$$

$$C_p(\omega) = C_s(\omega)\left[1 + tan^2\left(\frac{-Z'(\omega)}{Z''(\omega)}\right)\right] \quad (10)$$

The data obtained from EIS measurements can be transformed into Nyquist plots to demonstrate the relationship between real impedance *Z'* and imaginary impedance *Z''* [1]. The values for the real and imaginary part of capacitance are calculated from the equations (11) and (12):

$$C'(\omega) = -\frac{Z''(\omega)}{\omega|Z(\omega)|^2} \quad (11)$$

$$C''(\omega) = \frac{Z'(\omega)}{\omega|Z(\omega)|^2} \quad (12)$$

where $Z(\omega)$ is the complex impedance ($\omega = 2\pi f$). The characteristic time constant τ_1 is determined by the equation ($\tau_1 = \frac{1}{2\pi f_1}$).

The complex power values are determined as

$$S(\omega) = P(\omega) - jQ(\omega) \quad (13)$$

where the real part of power is determined as

$$P(\omega) = \omega C'(\omega)|\Delta E_{rms}|^2 \quad (14)$$

and the imaginary part of power as

$$Q(\omega) = \omega C'(\omega)|\Delta E_{rms}|^2 \quad (15)$$

with $|\Delta E_{rms}|^2 = \Delta E_{max}/\sqrt{2}$. A system with ideal capacitive behaviour has no real part of power because there exists only the reactive contribution to the complex power, therefore equation (9) shortens to

$$S(\omega) = jQ = -\frac{j\Delta E_{rms}^2}{|Z''|} = j\omega C \Delta E_{rms}^2 \quad (16)$$

Systems with ideal resistive behaviour have no imaginary part since it only dissipates energy and complex power is expressed as

$$S(\omega) = \frac{\Delta E_{rms}^2}{|Z'|} \quad (17)$$

Time constant calculated from complex power values $\tau_2 = \frac{1}{2\pi f_2}$.

5.7 Energy and Power Calculations

There is also a descriptive energy — power characterisation method called a Ragone plot which compares different energy storage devices by plotting energy density against power density on a logarithmic scale. The Ragone plot can give information about volumetric energy density as well as gravimetric energy density. It depends whether the calculation is made per unit mass or unit volume. The vertical axis illustrates how much energy is obtainable per unit mass and the horizontal axis depicts how quickly a system releases that energy. Calculating specific energy and specific power for an energy-storage device, the following equations are used respectively:

$$specific\ energy = \frac{E \times I \times t}{m}, \quad (18)$$

$$specific\ power = \frac{E \times I}{m}, \quad (19)$$

where E is potential (V), I is electric current (A), t is time (s) and m mass (kg) [74].

6. Experimental

6.1 Cell Assembly & Physical Characterization of Materials

The assembled test cell consisted of two electrodes, Zn foil electrode and carbon cloth electrode as negative and positive electrode, respectively. The cell was measured using different Zn salts in either acetonitrile or propylene carbonate solvents.

The two-electrode set-up had a polished Zn foil (Fig. 4) (with a thickness of 15 μm and a purity of 99.999% from Sigma-Aldrich) as one electrode and a microporous commercial carbon cloth (Fig. 5) as the other electrode (with a thickness of ~450 μm, Spectracarb™ 2225 type 900), which was cooled down in Ar atmosphere (10.25 mg cm^{-2} of mass loading). Initial characterization of carbon cloth electrode and Zn foil was done by SEM-EDS method.

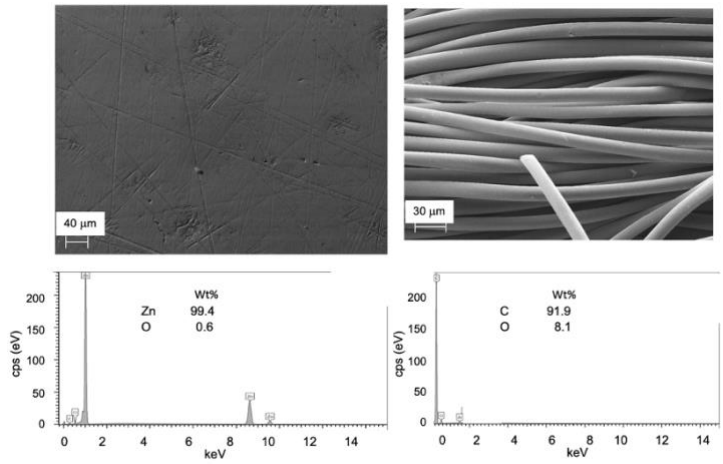

Figure 4. SEM image and SEM-EDS analysis of Zn foil.

Figure 5. SEM image and SEM-EDS analysis of carbon cloth.

For electrochemical testing purposes, 1 M non-aqueous electrolytes were prepared from 3 different Zn salts, $Zn(TFSI)_2$, $Zn(BF_4)_2$ and $Zn(OTf)_2$. All salts were from Sigma-Aldrich and had purities ranging from 95-98%. For solvents, acetonitrile (AN, HPLC Plus, ≥99.9%) and propylene carbonate (PC, anhydrous, 99.7%) from Sigma-Aldrich were employed. Measurements with $Zn(OTf)_2$ in PC were difficult to conduct and comparable results were not possible to obtain due to very low solubility (less than 0.2 M) of this electrolyte system.

Electrodes were separated by Whatman Grade GF/B Glass Microfiber (CAT No. 1821-090) separator with a thickness of approximately 0.8 mm. Moreover, no additional current collectors for both electrodes were applied. The assembly of the test cells (Fig. 6) (a stainless steel two-electrode cell from Hohsen Corp., Japan) was concluded inside a glovebox (Labmaster sb from MBraun, Germany) in argon atmosphere (99.9999%, Linde Gas, concentrations of O_2 and H_2O were below 0.1 ppm).

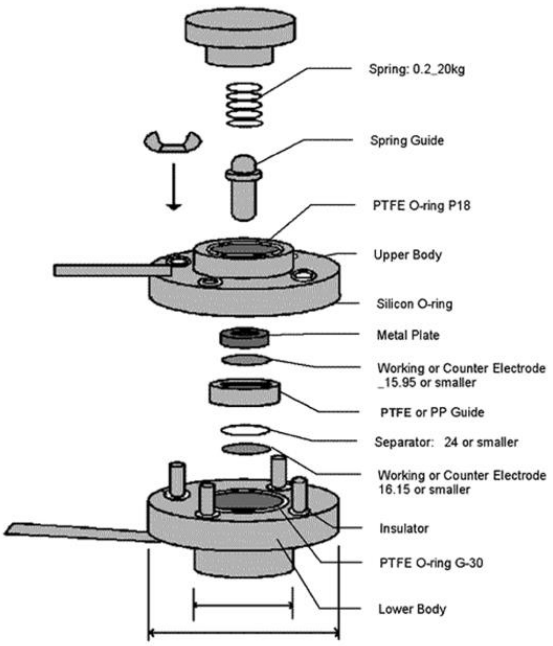

Figure 6. A scheme of the assembled test cell.

Zn foil electrode was prepared firstly by polishing. A chemical polishing solution (HNO_3 + H_2O) was used, then Zn electrode was treated with HCl aqueous solution and rinsed with MilliQ+ water. After, it was dried with ethanol (99.99%) and mechanically polished with diamond microcloth polishing cloth (Buehler), rinsed with ethanol and Ar saturated MilliQ+ water.

For physical characterization of electrode materials three different methods of analysis were used: low temperature N_2 sorption, XRD and Raman analysis. As seen from the N_2 adsorption-desorption isotherm graph (Fig. 7), the Spectracarb™ carbon electrode showed no hysteresis meaning that the carbon cloth is predominantly microporous with some minimal number of mesopores. Moreover, the carbon electrode had a high specific surface area (S_{BET} = 1450 m^2 g^{-1}) and total pore volume (V_{tot} = 0.68 cm^3 g^{-1}), which is usually associated with amorphous carbon structure.

Additionally, XRD and Raman spectroscopy (Fig. 8) also confirm that the carbon cloth electrode is amorphous with some graphitic regions. In XRD plot, short peak of 002 (at 24°), which is characteristic for graphite and 100/101 (at 44°) is affiliated with C materials without any crystalline order. Furthermore, there is a peak at 80° which proves the existence of some graphite-like regions. The Raman spectrum presented two distinctive bands at 1338 cm^{-1} and 1603 cm^{-1}. The high intensity disorder D-band at 1338 cm^{-1} again indicates its amorphous structure. Although, at 1603 cm^{-1} there is also a graphitic G-band which establishes the presence of graphitic areas.

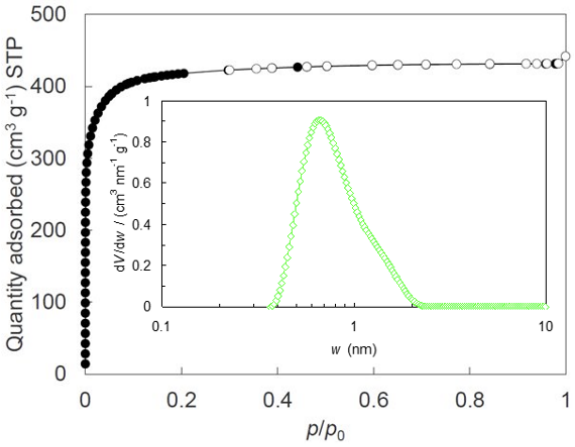

Figure 7. N_2 adsorption-desorption isotherm (inset: differential pore size distribution vs. pore size plot).

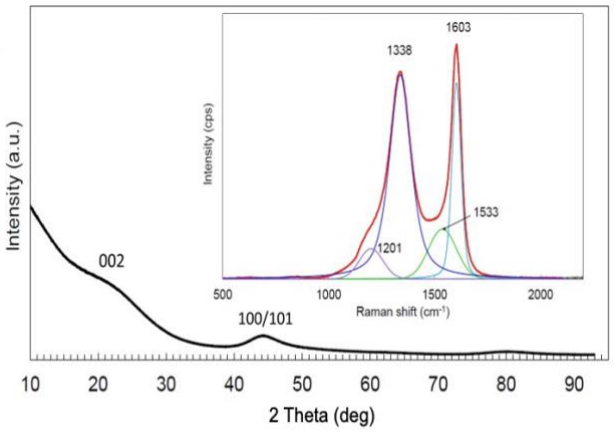

Figure 8. XRD and (inset: Raman spectroscopy) of carbon cloth electrode.

6.2 Cyclic Voltammetry Measurements

Assessing measured electrolyte systems $Zn(BF_4)_2$/AN, $Zn(BF_4)_2$/PC, $Zn(TFSI)_2$/AN and $Zn(TFSI)_2$/PC (Fig. 9-12) at low (1 mV s^{-1}) scan rate on specific capacitance vs cell potential graph demonstrates the superiority of AN over PC-based systems for respective Zn salts. For $Zn(BF_4)_2$/AN, a specific capacitance of ~150 F g^{-1} was attained, while $Zn(BF_4)_2$/PC achieved ~100 F g^{-1} at 2.0 V. In addition, $Zn(TFSI)_2$/AN had a specific capacitance ~75 F g^{-1} and $Zn(TFSI)_2$/PC achieved ~60 F g^{-1} at 2.0 V. Comparing the four abovementioned electrolyte

systems, a conclusion can be made that higher specific capacitances were achieved by AN-based systems, when comparing respective Zn-salts. Better performance of AN-based electrolyte in this case is most likely due to its more superior electrochemical stability and choice of solvent.

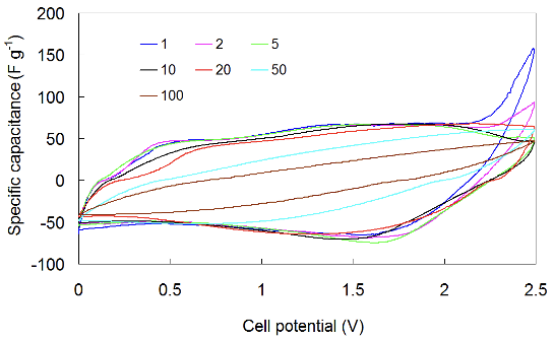

Figure 9. Cyclic voltammograms (CVs) at different scan rates for 1 M $Zn(TFSI)_2$/AN.

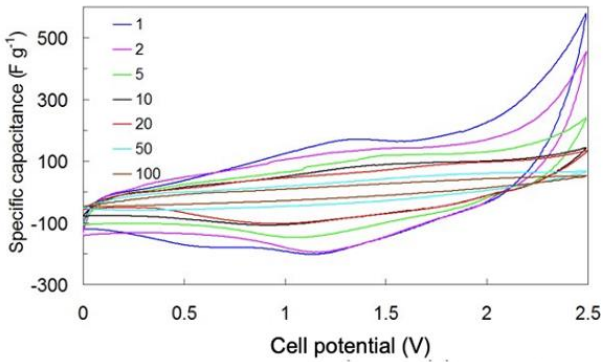

Figure 10. CVs expressed as specific capacitance vs. cell potential for 1 M $Zn(BF_4)_2$/AN.

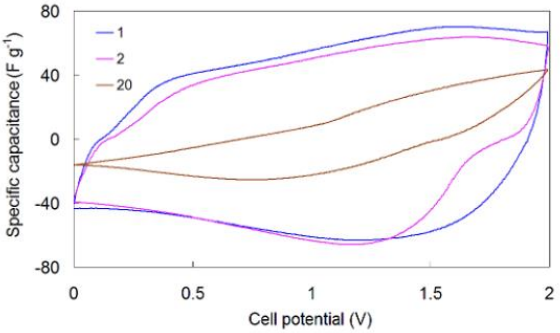

Figure 11. CVs expressed as specific capacitance vs. cell potential for 1 M $Zn(TFSI)_2$/PC.

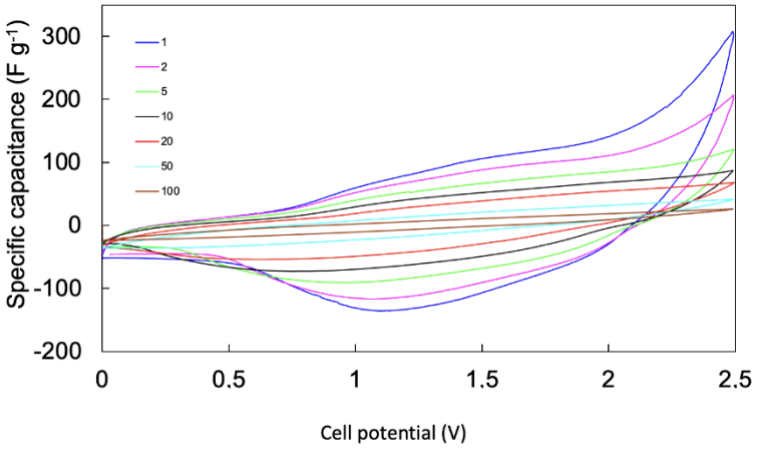

Figure 12. CVs expressed as specific capacitance vs. cell potential for 1 M $Zn(BF_4)_2$/PC.

Fig. 13 highlights all the measured electrolyte systems at the scan rate of 20 mV s^{-1}. Calculated specific capacitance curves show deviation from ideal symmetry because all assembled ZIHCs are hybrid capacitor systems and not EDLCs (ideal rectangular shapes are generally only visible in the case of EDLCs). Capacitance values are increasing in the order of: $Zn(TFSI)_2$/PC < $Zn(BF_4)_2$/PC < $Zn(TFSI)_2$/AN < $Zn(OTf)_2$/AN < $Zn(BF_4)_2$/AN. A conclusion can be made that because PC as a solvent is more viscous as AN, this in turn means more sluggish ion diffusion in PC solutions, resulting lower specific capacitances for these test cells. The CCCD measurements at fixed current densities were analysed within the potential region

from 0 to 2.0 V. Both charge and discharge capacitances were calculated using equation (2). Fig. 14 illustrates faster charging/discharging cycle times at 20 mA cm^{-2} for PC systems and longer cycle durations for AN solutions. Hence, Fig. 14 agrees with Fig. 13 and can therefore be presented as a supplementary graph to further validate specific capacitance comparisons between different electrolyte systems. Moreover, longer IR-drops observed on PC systems once more confirm that ion diffusion in those solutions are more restricted due to higher electrolyte resistance.

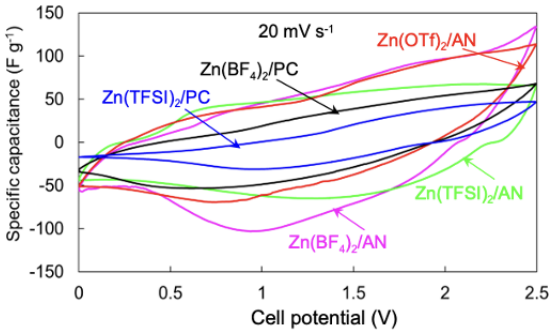

Figure 13. CVs expressed as specific capacitance vs. potential curves for all electrolyte systems at 20 mV s^{-1}.

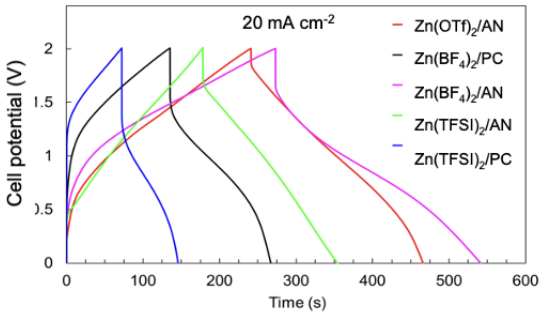

Figure 14. Constant current charge/discharge curves at 20 mA cm^{-2} for all measured 1 M Zn-salt test cells.

6.3 Electrochemical Impedance Spectroscopy Measurements

At cell potentials from 0-2.5 V (0.5 V being the potential step), ZIHC in different electrolyte solutions were measured within ac frequency ranging from 100 kHz to 1 mHz. Data is presented as Nyquist and Bode plots. The series resistance (R_s), series capacitance (C_s), parallel resistance (R_p) and parallel capacitance (C_p) were calculated from Nyquist plots (equations 7-10).

The comparison of $Zn(BF_4)_2$ salt in both AN and PC solvents indicates more superior electrochemical performance for acetonitrile-based electrolyte. Fig. 15-16 demonstrates that total series resistance R_s depends strongly on the used electrolyte. More compressed semi-circle for $Zn(BF_4)_2$/AN indicates lower charge transfer resistance for this system compared to $Zn(BF_4)_2$/PC. Due to higher electrolyte resistance and charge transfer resistance for the PC-based solution the overall internal resistance is much bigger, which leads to poor lifetime. Furthermore, at lower *ac* frequencies $Zn(BF_4)_2$/AN exhibits better capacitive behaviour than the respective dissolved zinc salt in PC solvent which deviates more heavily from the ideal capacitive system.

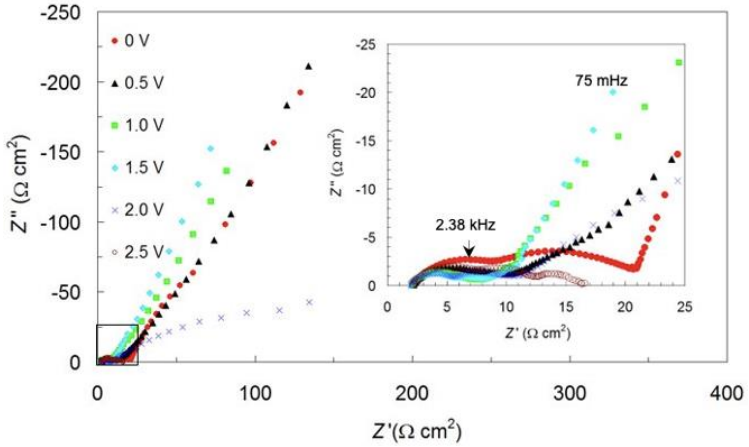

Figure 15. Nyquist plots for 1 M $Zn(BF_4)_2$/AN electrolyte at different cell potentials.

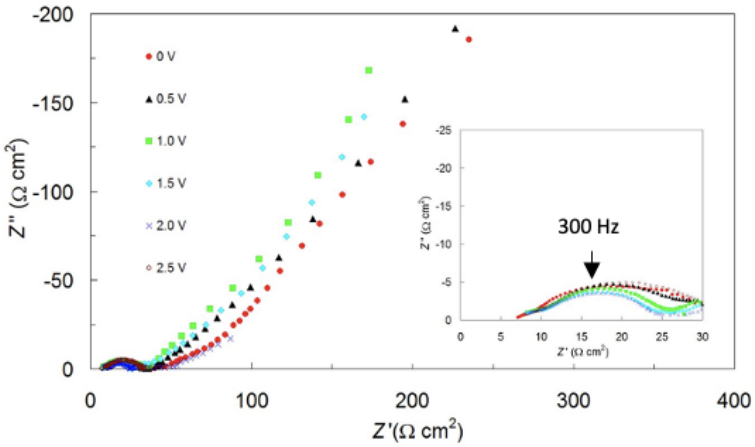

Figure 16. Nyquist plots for 1 M $Zn(BF_4)_2$/PC electrolyte at different cell potentials.

Further analysis on the Bode plot for $Zn(BF_4)_2$/AN (Fig. 17) displays the largest dependency on frequency in the region of 0.01 Hz to 0.1 Hz, hence being in the mass transfer/charge transfer limited kinetics region. In the potential region of 0 to 1.5 V at low *ac* frequencies phase angles from -50 to -70º were noticed, showing good capacitive behaviour for this system (phase angle of -90º for ideal capacitor).

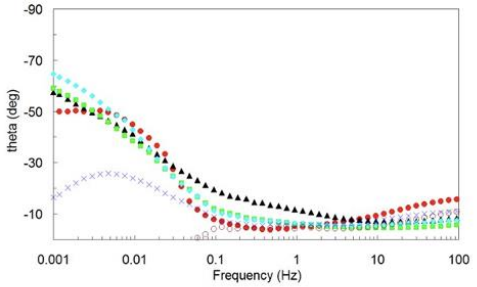

Figure 17. Bode phase angle plots for 1 M $Zn(BF_4)_2$/AN at different cell potentials.

Fig. 18 illustrates the ratio of parallel and series capacitance C_p/C_s vs log f at the frequency region of 0.001 Hz to 1 Hz. Measured ZIHCs cells are contingent on the applied potential and electrolyte system. This graph mostly has infographic value to indicate that these systems are hybrid and not ideal EDLCs because then the ratio must be close to -1. The ratio of C_p/C_s was the highest for $Zn(BF_4)_2$/AN compared to other systems, therefore this system's

behaviour is the most capacitive. Imaginary capacitance (*C´´*) vs *ac* frequency (Fig. 19) exhibits notable maximum frequencies at different cell potentials. From maximum frequencies, relaxation times for charging/charging cycles were calculated. Evidently, at 2.0 V maximum frequency point could not be found due to high resistance and faradaic processes inside the test cell. The measured hybrid system showed τ_1= 20-30 seconds of relaxation times for charging/discharging.

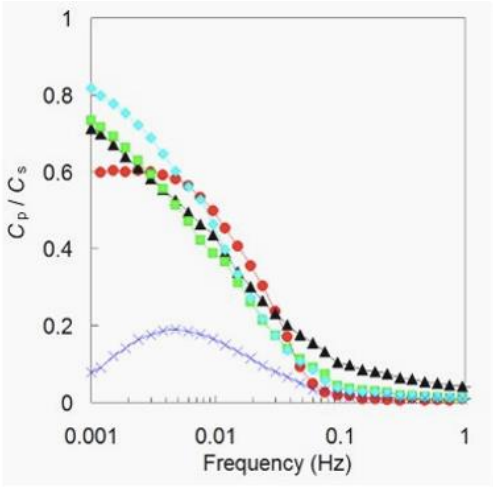

Figure 18. Ratio of parallel and series capacitance for 1 M $Zn(BF_4)_2$/AN.

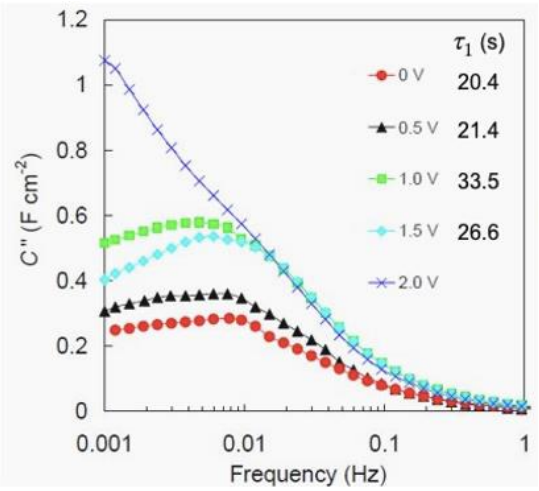

Figure 19. Imaginary part of capacitance for 1 M $Zn(BF_4)_2$/AN.

Fig 20. describes the dependency of normalised real part (|*P*|/|*S*|) and imaginary part (|*Q*|/|*S*|) of the complex power on *ac* frequency. Calculated charging/discharging time constants τ_2 from the interception points of the frequency lines depend on the cell potential and electrolyte solution. The measured ZIHC test cell $Zn(BF_4)_2$/AN showed the shortest charging/discharging time of 19.9 s at 1.5 V.

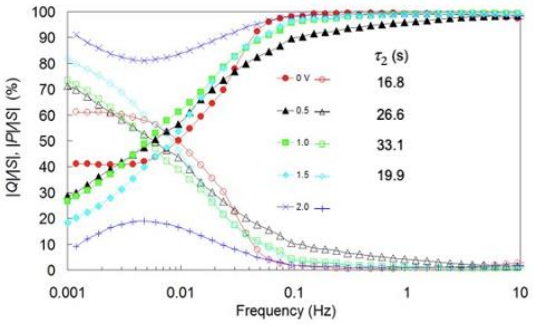

Figure 20. Normalized reactive power (|Q|/|S|) and active power (|P|/|S|) vs. ac frequency for 1 M $Zn(BF_4)_2$/AN.

Imaginary part of impedance vs. ac frequency graph (Fig. 21) at defined 0 V cell potential demonstrates nearly ideal (slope -1.0) adsorption step limited processes for certain electrolyte systems at low ac frequencies (f < 0.01 Hz). The closest systems to ideal adsorption are $Zn(TFSI)_2$/AN, $Zn(BF_4)_2$/AN and $Zn(BF_4)_2$/PC, with slopes of -0.95, -0.86 and -0.85 respectively. Impedance imaginary part vs. *ac* frequency plots (Fig. 21) at fixed cell potential show one linear region (slope from −0.95 to −0.71) at lower frequencies (f < 0.01 Hz) which is nearly equal to that for ideal adsorption step limited processes (slope −1.0). Only for $Zn(OTf)_2$/AN there is noticeable deviation from nearly ideally polarizable system. The shape of the log|−*Z″*|, log *f* plot is clearly dependent of the non-

aqueous electrolyte used. It demonstrates that the capacitance values are significantly dependent on the applied cell potential as well as on the used electrolyte. Surprisingly, the second linear region at higher frequencies, typically from 100 to 0.5 Hz (porous region) equal to that for semi-infinite mass transfer process (for ideal process the slope is −0.5) is missing. The biggest deviation from ideal capacitive system has been observed for $Zn(OTf)_2$/AN-based cell, where mass-transfer limited adsorption process in the entire studied frequency range can be seen in Fig. 22 (phase angle < −45°).

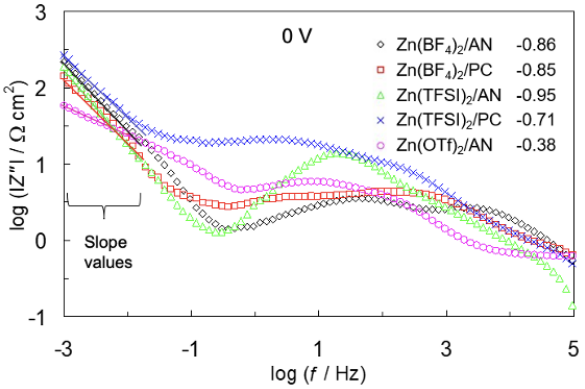

Figure 21. Imaginary part of impedance vs ac frequency for different electrolytes.

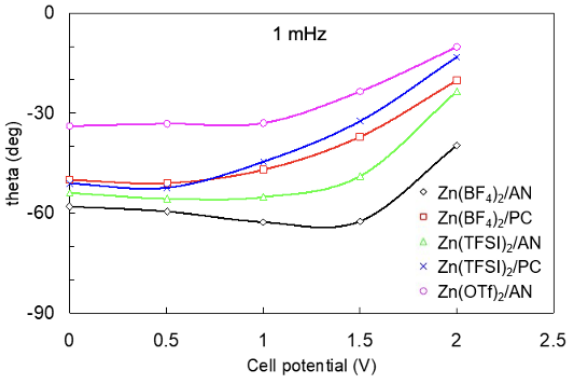

Figure 22. Phase angles at 1 mHz for different systems.

At 1 mHz, the series capacitance C_s values at different potentials (Fig. 23) were much better for AN-based systems. At 2 V, both $Zn(TFSI)_2$/PC and $Zn(BF_4)_2$/PC had capacitances of 120 F g^{-1} and 130 F g^{-1} respectively, while $Zn(BF_4)_2$/AN exhibited 165 F g^{-1} at the same cell potential. This validates that high energy density for ZIHS can be reached with abovementioned non-aqueous electrolyte solution.

Fig. 24 indicates that calculated series resistance R_s values at lower *ac* frequencies depend on the used electrolyte system. This graph again highlights poorer performance of PC-based systems compared to AN-based systems with $Zn(TFSI)_2$/PC having around 12 Ω cm^2 at 2 V. Much lower resistance values were calculated for both AN-based solutions where dissolved Zn salts $Zn(BF_4)$ and $Zn(TFSI)_2$ having 2 Ω cm^2 and 3 Ω cm^2 respectively at 2.0 V. These plots demonstrate that high power densities can be achieved for AN-based systems.

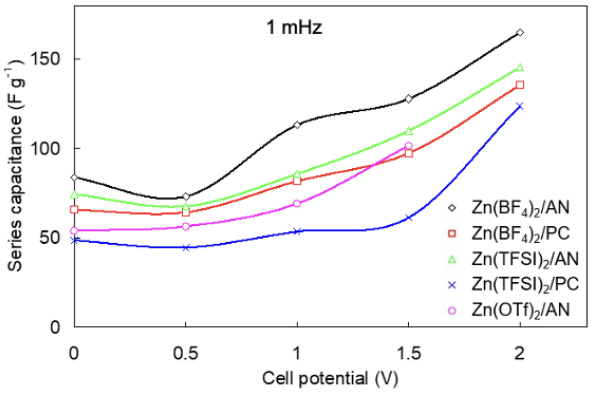

Figure 23. Series capacitance at 1 mHz for different systems.

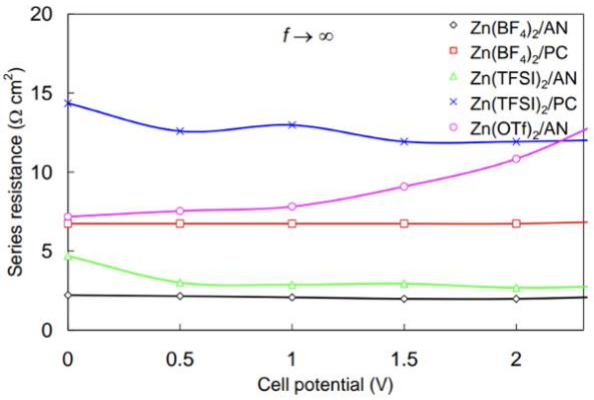

Figure 24. Series resistance vs cell potential for el. systems.

6.4 Ragone Plots

Ragone plots were measured (within the potential range from 2.0 to 0.5 V) and calculated for every AN-based electrolyte system $Zn(TFSI)_2$/AN, $Zn(BF_4)_2$/AN and $Zn(OTf)_2$/AN, as well as for two PC-based systems $Zn(TFSI)_2$/PC and $Zn(BF_4)_2$/PC. Measurements were not made for $Zn(OTf)_2$ in PC due to the insolubility of the zinc salt in PC solvent. The calculation of gravimetric densities was done by using the mass of both electrodes. The analysis of specific energy vs. specific power plot gives a good indication that higher energy densities were calculated for AN-based solutions, except for $Zn(OTf)_2$ in AN. This system in general exhibited poor electrochemical performance compared to other measured non-aqueous solutions. At lower power densities (1 kW kg^{-1}) the ranking of electrolyte systems are as follows: $Zn(BF_4)_2$/AN > $Zn(TFSI)_2$/AN > $Zn(BF_4)_2$/PC > $Zn(TFSI)_2$/PC > $Zn(OTf)_2$/AN (Fig. 25). $Zn(BF_4)_2$ and $Zn(TFSI)_2$ in acetonitrile solvent displayed specific energies of around 50-55 W h kg^{-1} at intermediate (2 kW kg^{-1}) power density values. The pair of PC systems did not achieve power densities over 3 kW kg^{-1}, compared to AN-based solutions that reached as high as 20 kW kg^{-1} of specific power. Again, highlighting better performance in favour of Zn-ion hybrid capacitor systems in acetonitrile.

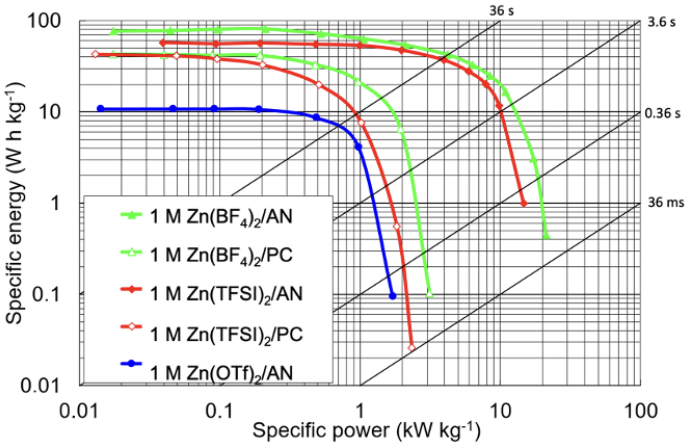

Figure 25. Ragone plots for measured non-aqueous ZIHC within potential range 2.0 to 0.5 V.

6.5 Coulombic & Energy Efficiencies

The stability of the electrolyte systems was measured through longer period of cycling with CCCD method at 2 A g^{-1}. All the examined test cells achieved over 3 000 cycles of lifetime and retained good electrochemical stability during the measurement. The coulombic efficiency was superb for all the ZIHC cells, maintaining 99.8-99.9%. The energy efficiencies were calculated using equations (3-4). The highest energy efficiency was calculated for $Zn(TFSI)_2$/AN nonaqueous solution with the value being 66.8% (Fig. 26). All the other electrolyte systems followed by the order of decreasing electrochemical stability $Zn(BF_4)_2$/PC > $Zn(TFSI)_2$/PC > $Zn(OTf)_2$/AN > $Zn(BF_4)_2$/AN.

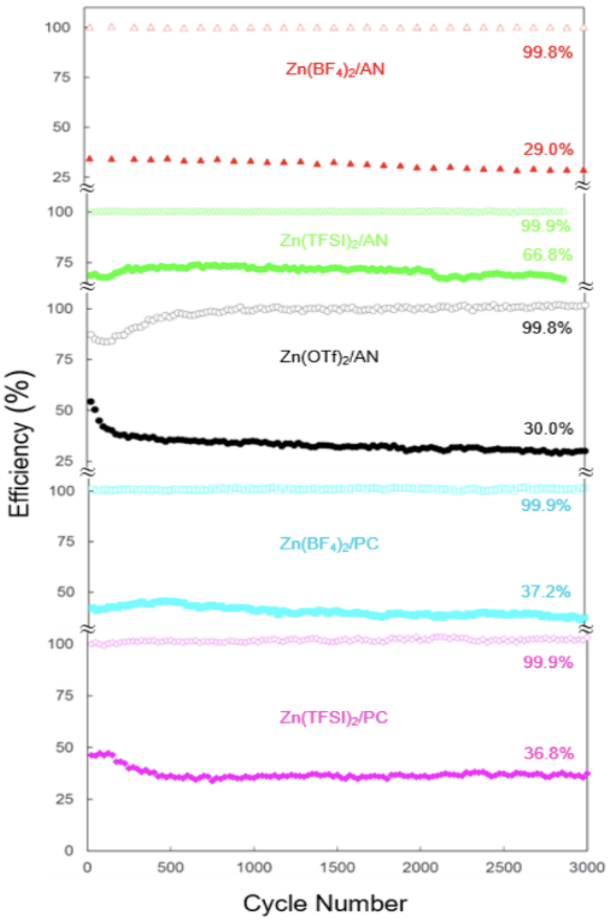

Figure 26. Coulombic and energy efficiency vs. cycle number at 2 A g^{-1}.

6.6 Lifetime Measurements

After cycling 1 M $Zn(TFSI)_2$/AN electrolyte system for 20 000 cycles, the coulombic ratio remained ~66% at 2 A g^{-1} of charge/discharge current (Fig. 27a). Zn foil electrode underwent surface colour change according to SEM-EDS analysis. The colour change was very likely due to altered chemical composition of the surface structure and formed SEI layer. Different amounts (wt.%) of O, C, S and F have been observed (Fig. 27b). Increased oxygen amounts and some small contents of sulphur and fluor are due to the electrolyte. Exhibited increase of carbon is because of the carbon cloth electrode. Moreover, after long term cycling no Zn dendrites were visible after opening the test cell. Dendrite growth from the surface of Zn electrode through the separator towards carbon electrode is commonly observed in aqueous-based electrolytes [72].

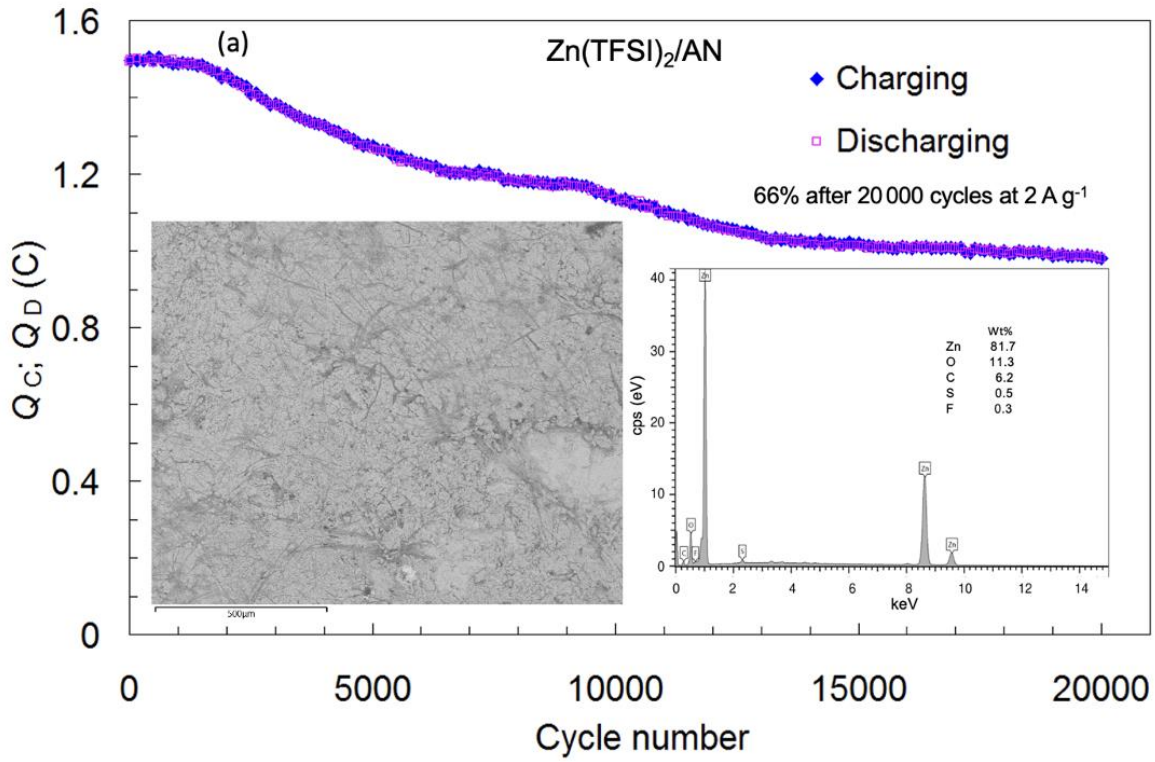

Figure 27a. Long 20 000 charge / discharge cycle lifetime measurement for 1 M $Zn(TFSI)_2$/AN test cell from 0 to 2.0 V cell potential and at current density of 2 A g^{-1}. Insets: (left) Zn electrode surface, (right) SEM-EDS analysis.

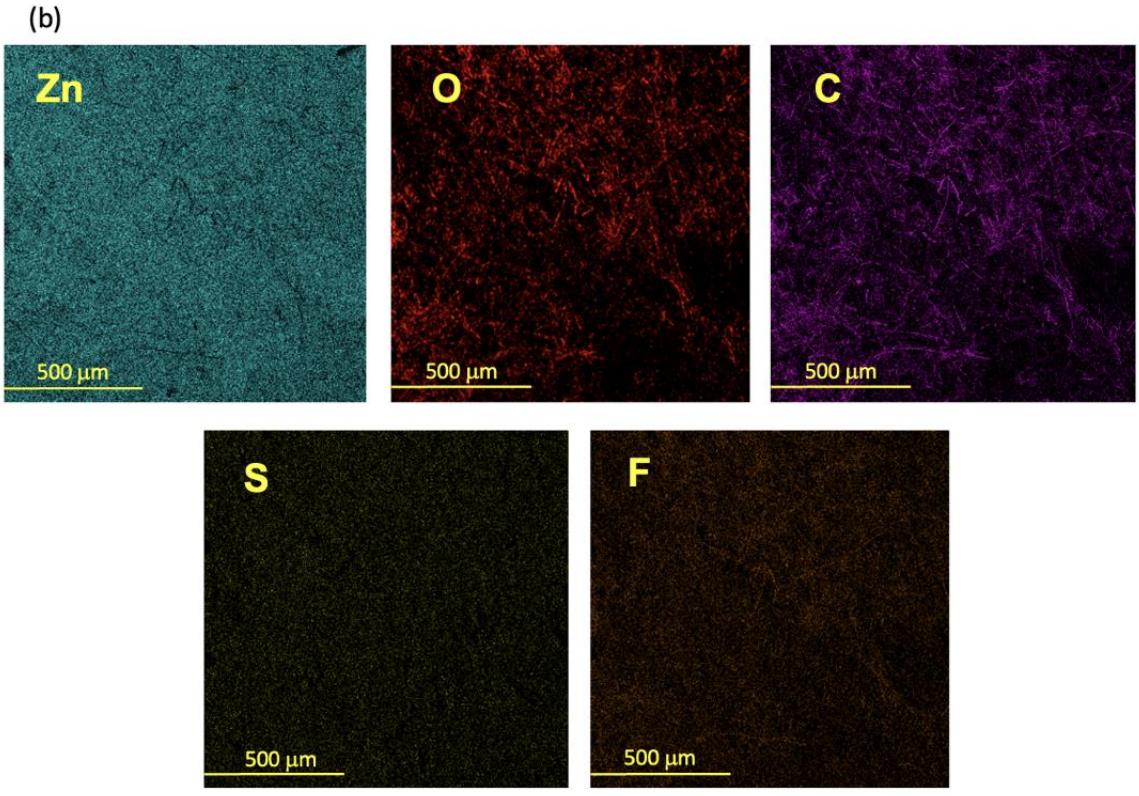

Figure 27b. Elemental mapping for Zn electrode after cycling.

7. Summary

We demonstrated that a cost effective and high energy density Zn-ion based hybrid supercapacitors (ZIHCs) are possible, using Zn as the negative electrode and commercially available SpectracarbTM 2225 activated carbon fabric as the positive electrode material. Various Zn cation-based 1 M acetonitrile and propylene carbonate electrolytes (zinc tetrafluoroborate, $Zn(BF_4)_2$; zinc di[bis(trifluoromethylsulfonyl)imide], $Zn(TFSI)_2$ and zinc trifluoromethanesulfonate, $Zn(OTf)_2$) were tested. Very high energy and power densities (~80 W h kg^{-1} and ~20 kW kg^{-1}) have been calculated for 1 M $Zn(BF_4)_2$/AN-based Zn-ion hybrid supercapacitor. Very good stability after 3000 cycles has been achieved for all measured test cells, demonstrating reasonably high energy efficiency value (66.8%) for $Zn(TFSI)_2$/AN-based ZIHC cell. Energy efficiencies for electrolytes decreased in the order of: $Zn(TFSI)_2$/AN > $Zn(BF_4)_2$/PC > $Zn(TFSI)_2$/PC > $Zn(OTf)_2$/AN > $Zn(BF_4)_2$/AN. The coulombic efficiency values are very high, nearly 99.8 – 99.9%. A long lifetime measurement for assembled 1 M $Zn(TFSI)_2$/AN-based ZIHC has shown good cycling and energy stability during 20 000 cycles. Thus, this work provides some insight into the strategy for designing effective non-aqueous Zn-ion hybrid supercapacitors.

References

[1] A. Yu, V. Chabot and J. Zhang, Electrochemical Supercapacitors for Energy Storage and Delivery Fundamentals and Applications, Boca Raton: CRC Press, 2013.

[2] S. S. Williamson, P. A. Cassani, S. Lukic and B. Blunier, Power Electronics Handbook (Third Edition*)*, Butterworth-Heinemann, 2011, pp. 1331-1356.

[3] M. Sarno, Nanotechnology in Energy Storage: The Supercapacitors, vol. 179, *Elsevier*, 2020, pp. 431-458.

[4] A. K. Samantara and S. Ratha, Metal-Ion Hybrid Capacitors for Energy Storage: A Balancing Strategy Toward Energy-Power Density, Springer, 2020.

[5] C. Liu, Z. Yu, D. Neff, A. Zhamu and B. Z. Jang, *Nano Letters*, vol. 10, no. 12, pp. 4863-4868, 2010.

[6] K. Ku, B. Kim, H. Chung and W. Kim, *Synthetic Metals*, vol. 160, no. 23-24, pp. 2613-2617, 2010.

[7] Y. Zhu, S. Murali, M. Stoller, K. Ganesh, W. Cai, P. Ferreira, A. Pirkle, R. Wallace, K. Cychosz, M. Thommes, D. Su, E. Stach and R. Ruoff, *Science*, vol. 332, no. 6037, pp. 1537-1541, 2011.

[8] Y. Shao, M. F. El-Kady, J. Sun, Y. Li, Q. Zhang, M. Zhu, H. Wang, B. Dunn and R. B. Kaner, *Chem. Rev.*, vol. 118, no. 18, pp. 9233-9280, 2018.

[9] V. Khomenko, E. Raymundo-Pinero and F. E., Appl. Phys. A, vol. 82, pp. 567-573, 2006.

[10] J. P. Zheng, *Electrochem. Solid-State Lett.*, vol. 2, pp. 359-361, 1999.

[11] V. Khomenko, E. Raymundo-Pinero and F. Beguin, *J. Power Sources*, vol. 153, pp. 183-190, 2006.

[12] W. Wei, X. Cui, W. Chen and D. G. Ivey, *Chem. Soc. Rev.*, vol. 40, pp. 1697-1721, 2011.

[13] B. Vidyadharan, R. A. Aziz, I. I. Minson, G. M. Anil Kumar, J. Ismail, M. M. Yusoff and R. Jose, *J. Power Sources*, vol. 270, pp. 526-535, 2014.

[14] J. Huang, P. Xu, D. Cao, X. Zhou, S. Yang, Y. Li and G. Wang, *J. Power Sources*, vol. 246, pp. 371-376, 2014.

[15] S. Gao, Y. Sun, F. Lei, L. Liang, J. Liu, W. Bi, B. Pan and Y. Xie, *Angew. Chem, Int. Ed.*, vol. 53, pp. 12789-12793, 2014.

[16] X. Wang, C. Yan, A. Sumboja and P. S. Lee, *Nano Energy*, vol. 3, pp. 119-126, 2014.

[17] C. Zhou, Y. Zhang, Y. Li and J. Liu, *Nano Lett.*, vol. 13, pp. 2078-2085, 2013.

[18] L. Shen, J. Wang, G. Xu, H. Li, H. Dou and X. Zhang, *Adv. Energy Matter*, vol. 5, no. 3, 2015.

[19] A. Singh, A. J. Roberts, R. C. T. Slade and A. Chandra, *J. Mater. Chem. A*, no. 39, 2014.

[20] K. C. Ng, S. Zhang, C. Peng and G. Z. Chen, *J. Electrochem. Soc.*, vol. 156, no. 11, pp. 846-853, 2009.

[21] Q. Qu, Y. Zhu, X. Gao and Y. Wu, *Adv. Energy Mater*, vol. 2, no. 8, pp. 950-955, 2012.

[22] B. Li, J. Zheng and H. Zhang, *Adv. Mater*, vol. 30, no. 17, 2018.

[23] Y.-E. Zhu, L. Yang and X. Zhou, *J. Mater Chem. A.*, no. 20, 2017.

[24] J. Muldoon, C. B. Bucur and T. Gregory, *Chem. Rev.*, vol. 114, no. 23, pp. 11683-11720, 2014.

[25] G. A. Elia, K. V. Kraychyk, M. V. Kovalenko, J. Chacon, A. Holland and R. G. A. Wills, *Journal of Power Sources*, vol. 481, 2021.

[26] Pure Energy Minerals, 2023. [Online]. Available:https://pureenergyminerals.com/overview/why-lithium/.

[27] L. Zhang, D. P. Wilkinson, Z. Chen and J. Zhang, Lithium-Ion Supercapacitors: Fundamentals and Energy Applications, Boca Raton: CRC Press, 2018.

[28] N. Xu, X. Sun and X. Zhang, *RSC Adv.*, no. 114, 2015.

[29] C. Zhang, W. Lv and X. Xie, *Carbon*, vol. 62, pp. 11-24, 2013.

[30] E. Lim, H. Kim and C. Jo, *ACS Nano*, vol. 8, no. 9, pp. 8968-8978, 2014.

[31] Z. Chen, V. Augustyn and J. Wen, *Adv. Mater*, vol. 23, no. 6, pp. 791-795, 2011.

[32] X. Zhang, L. Wang and W. Liu, *ACS Omega*, vol. 5, no. 1, pp. 75-82, 2020.

[33] R. Yi, S. Chen and J. Song, *Adv. Funct. Mater*, vol. 24, no. 47, pp. 7433-7439, 2014.

[34] A. Bauer, J. Song and S. Vail, *Adv. Energy Mater*, vol. 8, no. 17, 2018.

[35] P. Ge, H. Hou and C. E. Banks, *Energy Storage Mater*, vol. 12, pp. 310-323, 2018.

[36] R. Thangavel, K. Kaliyappan and D.-U. Kim, *Chem. Mater.*, vol. 29, no. 17, pp. 7122-7130, 2017.

[37] J.-T. Han and J. B. Goodenough, *Chem. Mater*, vol. 23, no. 15, pp. 3404-3407, 2011.

[38] Y. Dong, Z.-S. Wu and S. Zheng, *ACS Nano*, vol. 11, no. 5, pp. 4792-4800, 2017.

[39] Y. Wang, Z. Zhang and G. Wang, *Nanoscale Horizons*, no. 6, 2019.

[40] Z. Zhang, M. Li and Y. Gao, *Adv. Funct. Mater*, vol. 28, no. 36, 2018.

[41] Q. Zhao, J. Wang and Y. Lu, *Angew Chemie Int. Ed.*, vol. 55, no. 40, pp. 12528-12532, 2016.

[42] J. M. Sangster, *J. Phase Equilibria Diffus.*, vol. 31, pp. 68-72, 2010.

[43] M. Wang, C. Jiang and S. Zhang, *Nat. Chem.*, vol. 10, pp. 667-672, 2018.

[44] C. Lee and S.-K. Jeong, *Chemistry Letters*, vol. 45, no. 12, pp. 1447-1449, 2016.

[45] R. Zhang and C. Ling, *MRS Energy Sustain.*, vol. 3, no. E1, 2016.

[46] S. Liu, J. J. Hu, N. F. Yan, G. L. Pan, G. R. Li and X. P. Gao, *Energ. Environ. Sci.*, no. 12, 2012.

[47] A. Holland, R. D. McKerracher, A. Cruden and R. G. A. Willis, *J. Appl. Electrochem.*, vol. 48, pp. 243-250, 2018.

[48] J. Jin, X. Geng and Q. Chen, *Nano-Micro Lett.*, vol. 14, no. 64, 2022.

[49] X. Gong, J. Chen and P. S. Lee, *Batteries & Supercaps*, vol. 4, no. 10, pp. 1529-1546, 2021.

[50] J. Hao, X. Li, X. Zeng, D. Li, J. Mao and Z. Guo, *Energy & Environmental Science*, no. 11, 2020.

[51] S. Siahrostami, V. Tripkovic, K. T. Lundgaard, K. E. Jensen, H. A. Hansen, J. S. Hummelshoj, J. S. G. Myrdal, T. Vegge, J. K. Norskov and J. Rossmeisl, *Phys. Chem. Chem. Phys.*, no. 15, p. 6416, 2013.

[52] Z. Zhao, J. Zhao, Z. Hu, J. Li, J. Li, Y. Zhang, C. Wang and G. Cui, *Energy & Environmental Science*, no. 6, 2019.

[53] Z. Cao, P. Zhuang, X. Zhang, M. Ye, J. Shen and P. M. Ajayan, *Advanced Energy Materials*, vol. 10, no. 30, 2020.

[54] X. Zhang, Z. Pei, C. Wang, Z. Yuan, L. Wei, Y. Pan, A. Mahmood, Q. Shao and Y. Chen, *Small*, vol. 15, no. 47, 2019.

[55] L. Dong, W. Yang, W. Yang, H. Tian, Y. Huang, X. Wang, C. Xu, C. Wang, F. Kang and G. Wang, *Chemical Engineering Journal*, vol. 384, 2020.

[56] C. Wang, Z. Pei, Q. Meng, C. Zhang, S. Xiao, Z. Yuan, S. Wang and Y. Chen, *Angewandte Chemie International Edition*, vol. 60, no. 2, pp. 990-997, 2020.

[57] J. Hao, J. Long, B. Li, X. Li, S. Zhang, F. Yang, X. Zeng, Z. Yang, W. K. Pang and Z. Guo, *Advanced Functional Materials*, vol. 29, no. 34, 2019.

[58] Y.-G. Lee and G.-H. An, *ACS Appl. Mater. Interfaces*, vol. 12, no. 37, pp. 41342-41349, 2020.

[59] Y. Tian, R. Amal and D.-W. Wang, *Front. Energy Res.*, vol. 4, 2016.

[60] X. Ma, J. Cheng, L. Dong, W. Liu, J. Mou, L. Zhao, J. Wang, D. Ren, J. Wu, C. Xu and F. Kang, *Energy Storage Materials*, vol. 20, pp. 335-342, 2019.

[61] Q. Yang, Z. Huang, X. Li, Z. Liu, H. Li, G. Liang, D. Wang, Q. Huang, S. Zhang, S. Chen and C. Zhi, *ACS Nano*, vol. 13, no. 7, pp. 8275-8283, 2019.

[62] H. Cong, Z. Xin, X. Yali, Z. Yan, Y. Yujie, H. Aiping, T. Qunli, S. Xianyin, J. Changzhong and C. Xiaohua, *ACS Sustainable Chemistry & Engineering*, vol. 8, no. 42, pp. 16028-16036, 2020.

[63] Z. Huang, A. Chen, F. Mo, G. Liang, X. Li, Q. Yang, Y. Guo, Z. Chen, Q. Li, B. Dong and C. Zhi, *Advanced Energy Materials*, vol. 10, no. 24, 2020.

[64] W. Kao-ian, A. A. Mohamad, W.-R. Liu, R. Pornprasertsuk, S. Siwamogsatham and S. Kheawhom, *Batteries & Supercaps*, vol. 5, no. 5, 2022.

[65] S.-D. Han, N. N. Rajput, X. Qu, B. Pan, M. He, M. S. Ferrandon, C. Liao, K. A. Persson and A. K. Burrell, *ACS Appl. Mater. Interfaces*, vol. 8, no. 5, pp. 3021-3031, 2016.

[66] A. S. Etman, M. Carboni, J. Sun and R. Younesi, *Energy Technol.*, vol. 8, no. 9, 2020.

[67] L. Ma, M. A. Schroeder, T. P. Pollard, O. Borodin, M. S. Ding, R. Sun, L. Cao, J. Ho, D. R. Baker, C. Wang and K. Xu, *Energy Environ. Mater.*, vol. 3, no. 4, pp. 516-521, 2020.

[68] A. Naveed, H. Yang, Y. Shao, J. Yang, N. Yanna, J. Liu, S. Shi, L. Zhang, A. Ye, B. He and J. Wang, *Adv. Mater.*, vol. 31, no. 36, 2019.

[69] T. Romann, Raman Spectroscopy: Testing and investigation methods in materials science - unpublished study material.

[70] M. Pohl, Süsiniknanotorude mõju titaankarbiidist sünteesitud süsinikmaterjalidel põhinevate superkondensaatorite karakteristikutele, University of Tartu, Tartu, 2016.

[71] K. S. W. Sing, *Studies in Surface Science and Catalysis*, vol. 62, pp. 1-9, 1991.

[72] J. Eskusson, T. Thomberg, T. Romann, K. Lust, E. Lust and A. Jänes, *J. Solid State Electrochemistry*, no. 25, pp. 2869-2880, 2021.

[73] M. Härmas, Impact of activated carbon microstructure and porosity on electrochemical performance of electrical double-layer capacitors, University of Tartu Press, Tartu, 2020.

[74] T. Christen and M. W. Carlen, *Journal of Power Sources*, vol. 91, pp. 210-216, 2000.

[75] H. Wang, M. Wang and Y. Tang, *En. Stor. Mat.*, vol. 13, pp. 1-7, 2018.

[76] V. Aravindan, J. Gnanaraj, Y.-S. Lee and S. Madhavi, *Chem. Rev.*, vol. 114, no. 23, pp. 11619-11635, 2016.

[77] M. Javed, S. Asim, T. Najam, M. Khalid, I. Hussain, A. Ahmad, M. A. Assiri, W. Han, *Carbon Energy*, vol. 5, no. 1, p. 4, 2023.

Acknowledgements

First of all, I am extremely thankful for the help and guidance my supervisor Assoc. Prof. Alar Jänes gave me during the whole process, starting from explaining physical characterization methods and electrochemistry to writing the thesis. In addition, big thanks to Research Fellow Jaanus Eskusson for helping me in the laboratory to prepare test cells and giving me invaluable experience in working in laboratory conditions. This knowledge that I have gained has been very helpful in my current line of work.

Secondly, this work was supported by the EU through the European Regional Development Fund under projects TK141 "Advanced materials and high-technology devices for energy recuperation systems" (2014–2020.4.01.15–0011) and Personal Research Grant PRG 676. The author would also like to thank Miriam Koppel, Tavo Romann, Kalle Kirsimäe and Jaan Aruväli at University of Tartu for gas sorption, Raman, SEM-EDS and XRD measurements, respectively.

Non-exclusive licence to reproduce the thesis and make the thesis public

I, Karl-Sten Põder,

1. grant the University of Tartu a free permit (non-exclusive licence) to

reproduce, for the purpose of preservation, including for adding to the DSpace digital archives until the expiry of the term of copyright, my thesis

High energy density Zn-ion hybrid capacitor using non-aqueous electrolytes,

supervised by Alar Jänes and Jaanus Eskusson.

2. I grant the University of Tartu a permit to make the thesis specified in point 1 available to the public via the web environment of the University of Tartu, including via the DSpace digital archives, under the Creative Commons licence CC BY NC ND 4.0, which allows, by giving appropriate credit to the author, to reproduce, distribute the work and communicate it to the public, and prohibits the creation of derivative works and any commercial use of the work until the expiry of the term of copyright.

3. I am aware of the fact that the author retains the rights specified in points 1 and 2.

4. I confirm that granting the non-exclusive licence does not infringe other persons' intellectual property rights or rights arising from the personal data protection legislation.

Karl-Sten Põder
19/05/2023